# Inclusive Measurement of Diffractive Deep-inelastic *ep* Scattering

## H1 Collaboration

### Abstract

A measurement is made of the cross section for the process $ep \rightarrow eXY$ in deep-inelastic scattering with the H1 detector at HERA. The cross section is presented in terms of a differential structure function $F_2^{D(3)}(x_{\mathbb{P}}, \beta, Q^2)$ of the proton over the kinematic range $4.5 < Q^2 < 75\,\text{GeV}^2$. The dependence of $F_2^{D(3)}$ on $x_{\mathbb{P}}$ is found to vary with $\beta$, demonstrating that a factorisation of $F_2^{D(3)}$ with a single diffractive flux independent of $\beta$ and $Q^2$ is not tenable. An interpretation in which a leading diffractive exchange and a subleading reggeon contribute to $F_2^{D(3)}$ reproduces well the $x_{\mathbb{P}}$ dependence of $F_2^{D(3)}$ with values for the pomeron and subleading reggeon intercepts of $\alpha_{\mathbb{P}}(0) = 1.203 \pm 0.020(\text{stat.}) \pm 0.013(\text{sys.})^{+0.030}_{-0.035}(\text{model})$ and $\alpha_{\mathbb{R}}(0) = 0.50 \pm 0.11(\text{stat.}) \pm 0.11(\text{sys.})^{+0.09}_{-0.10}(\text{model})$, respectively. A fit is performed of the data using a QCD motivated model, in which parton distributions are assigned to the leading and subleading exchanges. In this model, the majority of the momentum of the pomeron must be carried by gluons in order for the data to be well described.

C. Adloff[35], S. Aid[13], M. Anderson[23], V. Andreev[26], B. Andrieu[29], V. Arkadov[36], C. Arndt[11], I. Ayyaz[30], A. Babaev[25], J. Bähr[36], J. Bán[18], P. Baranov[26], E. Barrelet[30], R. Barschke[11], W. Bartel[11], U. Bassler[30], M. Beck[14], H.-J. Behrend[11], C. Beier[16], A. Belousov[26], Ch. Berger[1], G. Bernardi[30], G. Bertrand-Coremans[4], R. Beyer[11], P. Biddulph[23], J.C. Bizot[28], K. Borras[8], F. Botterweck[27], V. Boudry[29], S. Bourov[25], A. Braemer[15], W. Braunschweig[1], V. Brisson[28], D.P. Brown[23], W. Brückner[14], P. Bruel[29], D. Bruncko[18], C. Brune[16], J. Bürger[11], F.W. Büsser[13], A. Buniatian[4], S. Burke[19], G. Buschhorn[27], D. Calvet[24], A.J. Campbell[11], T. Carli[27], M. Charlet[11], D. Clarke[5], B. Clerbaux[4], S. Cocks[20], J.G. Contreras[8], C. Cormack[20], J.A. Coughlan[5], M.-C. Cousinou[24], B.E. Cox[23], G. Cozzika[9], D.G. Cussans[5], J. Cvach[31], S. Dagoret[30], J.B. Dainton[20], W.D. Dau[17], K. Daum[40], M. David[9], C.L. Davis[19,41], A. De Roeck[11], E.A. De Wolf[4], B. Delcourt[28], M. Dirkmann[8], P. Dixon[19], W. Dlugosz[7], K.T. Donovan[21], J.D. Dowell[3], A. Droutskoi[25], J. Ebert[35], T.R. Ebert[20], G. Eckerlin[11], V. Efremenko[25], S. Egli[38], R. Eichler[37], F. Eisele[15], E. Eisenhandler[21], E. Elsen[11], M. Erdmann[15], A.B. Fahr[13], L. Favart[28], A. Fedotov[25], R. Felst[11], J. Feltesse[9], J. Ferencei[18], F. Ferrarotto[33], K. Flamm[11], M. Fleischer[8], M. Flieser[27], G. Flügge[2], A. Fomenko[26], J. Formánek[32], J.M. Foster[23], G. Franke[11], E. Gabathuler[20], K. Gabathuler[34], F. Gaede[27], J. Garvey[3], J. Gayler[11], M. Gebauer[36], R. Gerhards[11], A. Glazov[36], L. Goerlich[6], N. Gogitidze[26], M. Goldberg[30], B. Gonzalez-Pineiro[30], I. Gorelov[25], C. Grab[37], H. Grässler[2], T. Greenshaw[20], R.K. Griffiths[21], G. Grindhammer[27], A. Gruber[27], C. Gruber[17], T. Hadig[1], D. Haidt[11], L. Hajduk[6], T. Haller[14], M. Hampel[1], W.J. Haynes[5], B. Heinemann[11], G. Heinzelmann[13], R.C.W. Henderson[19], S. Hengstmann[38], H. Henschel[36], I. Herynek[31], M.F. Hess[27], K. Hewitt[3], K.H. Hiller[36], C.D. Hilton[23], J. Hladký[31], M. Höppner[8], D. Hoffmann[11], T. Holtom[20], R. Horisberger[34], V.L. Hudgson[3], M. Hütte[8], M. Ibbotson[23], Ç. İşsever[8], H. Itterbeck[1], M. Jacquet[28], M. Jaffre[28], J. Janoth[16], D.M. Jansen[14], L. Jönsson[22], D.P. Johnson[4], H. Jung[22], P.I.P. Kalmus[21], M. Kander[11], D. Kant[21], U. Kathage[17], J. Katzy[15], H.H. Kaufmann[36], O. Kaufmann[15], M. Kausch[11], S. Kazarian[11], I.R. Kenyon[3], S. Kermiche[24], C. Keuker[1], C. Kiesling[27], M. Klein[36], C. Kleinwort[11], G. Knies[11], J.H. Köhne[27], H. Kolanoski[39], S.D. Kolya[23], V. Korbel[11], P. Kostka[36], S.K. Kotelnikov[26], T. Krämerkämper[8], M.W. Krasny[6,30], H. Krehbiel[11], D. Krücker[27], A. Küpper[35], H. Küster[22], M. Kuhlen[27], T. Kurča[36], B. Laforge[9], R. Lahmann[11], M.P.J. Landon[21], W. Lange[36], U. Langenegger[37], A. Lebedev[26], F. Lehner[11], V. Lemaitre[11], S. Levonian[29], M. Lindstroem[22], J. Lipinski[11], B. List[11], G. Lobo[28], G.C. Lopez[12], V. Lubimov[25], D. Lüke[8,11], L. Lytkin[14], N. Magnussen[35], H. Mahlke-Krüger[11], E. Malinovski[26], R. Maraček[18], P. Marage[4], J. Marks[15], R. Marshall[23], J. Martens[35], G. Martin[13], R. Martin[20], H.-U. Martyn[1], J. Martyniak[6], T. Mavroidis[21], S.J. Maxfield[20], S.J. McMahon[20], A. Mehta[5], K. Meier[16], P. Merkel[11], F. Metlica[14], A. Meyer[13], A. Meyer[11], H. Meyer[35], J. Meyer[11], P.-O. Meyer[2], A. Migliori[29], S. Mikocki[6], D. Milstead[20], J. Moeck[27], F. Moreau[29], J.V. Morris[5], E. Mroczko[6], D. Müller[38], K. Müller[11], P. Murín[18], V. Nagovizin[25], R. Nahnhauer[36], B. Naroska[13], Th. Naumann[36], I. Négri[24], P.R. Newman[3], D. Newton[19], H.K. Nguyen[30], T.C. Nicholls[3], F. Niebergall[13], C. Niebuhr[11], Ch. Niedzballa[1], H. Niggli[37], G. Nowak[6], T. Nunnemann[14], H. Oberlack[27], J.E. Olsson[11], D. Ozerov[25], P. Palmen[2], E. Panaro[11], A. Panitch[4], C. Pascaud[28], S. Passaggio[37], G.D. Patel[20], H. Pawletta[2], E. Peppel[36], E. Perez[9], J.P. Phillips[20], A. Pieuchot[24], D. Pitzl[37], R. Pöschl[8], G. Pope[7], B. Povh[14],

1

K. Rabbertz[1], P. Reimer[31], H. Rick[8], S. Riess[13], E. Rizvi[11], E. Rizvi[21], P. Robmann[38], R. Roosen[4], K. Rosenbauer[1], A. Rostovtsev[30], F. Rouse[7], C. Royon[9], K. Rüter[27], S. Rusakov[26], K. Rybicki[6], D.P.C. Sankey[5], P. Schacht[27], J. Scheins[1], S. Schiek[11], S. Schleif[16], P. Schleper[15], W. von Schlippe[21], D. Schmidt[35], G. Schmidt[11], L. Schoeffel[9], A. Schöning[11], V. Schröder[11], E. Schuhmann[27], H.-C. Schultz-Coulon[11], B. Schwab[15], F. Sefkow[38], A. Semenov[25], V. Shekelyan[11], I. Sheviakov[26], L.N. Shtarkov[26], G. Siegmon[17], U. Siewert[17], Y. Sirois[29], I.O. Skillicorn[10], T. Sloan[19], P. Smirnov[26], M. Smith[20], V. Solochenko[25], Y. Soloviev[26], A. Specka[29], J. Spiekermann[8], S. Spielman[29], H. Spitzer[13], F. Squinabol[28], P. Steffen[11], R. Steinberg[2], J. Steinhart[13], B. Stella[33], A. Stellberger[16], J. Stiewe[16], K. Stolze[36], U. Straumann[15], W. Struczinski[2], J.P. Sutton[3], M. Swart[16], S. Tapprogge[16], M. Taševský[32], V. Tchernyshov[25], S. Tchetchelnitski[25], J. Theissen[2], G. Thompson[21], P.D. Thompson[3], N. Tobien[11], R. Todenhagen[14], P. Truöl[38], J. Zálešák[32], G. Tsipolitis[37], J. Turnau[6], E. Tzamariudaki[11], P. Uelkes[2], A. Usik[26], S. Valkár[32], A. Valkárová[32], C. Vallée[24], P. Van Esch[4], P. Van Mechelen[4], D. Vandenplas[29], Y. Vazdik[26], P. Verrecchia[9], G. Villet[9], K. Wacker[8], A. Wagener[2], M. Wagener[34], R. Wallny[15], T. Walter[38], B. Waugh[23], G. Weber[13], M. Weber[16], D. Wegener[8], A. Wegner[27], T. Wengler[15], M. Werner[15], L.R. West[3], S. Wiesand[35], T. Wilksen[11], S. Willard[7], M. Winde[36], G.-G. Winter[11], C. Wittek[13], M. Wobisch[2], H. Wollatz[11], E. Wünsch[11], J. Žáček[32], D. Zarbock[12], Z. Zhang[28], A. Zhokin[25], P. Zini[30], F. Zomer[28], J. Zsembery[9], and M. zurNedden[38],


[1] I. Physikalisches Institut der RWTH, Aachen, Germany[a]
[2] III. Physikalisches Institut der RWTH, Aachen, Germany[a]
[3] School of Physics and Space Research, University of Birmingham, Birmingham, UK[b]
[4] Inter-University Institute for High Energies ULB-VUB, Brussels; Universitaire Instelling Antwerpen, Wilrijk; Belgium[c]
[5] Rutherford Appleton Laboratory, Chilton, Didcot, UK[b]
[6] Institute for Nuclear Physics, Cracow, Poland[d]
[7] Physics Department and IIRPA, University of California, Davis, California, USA[e]
[8] Institut für Physik, Universität Dortmund, Dortmund, Germany[a]
[9] DSM/DAPNIA, CEA/Saclay, Gif-sur-Yvette, France
[10] Department of Physics and Astronomy, University of Glasgow, Glasgow, UK[b]
[11] DESY, Hamburg, Germany[a]
[12] I. Institut für Experimentalphysik, Universität Hamburg, Hamburg, Germany[a]
[13] II. Institut für Experimentalphysik, Universität Hamburg, Hamburg, Germany[a]
[14] Max-Planck-Institut für Kernphysik, Heidelberg, Germany[a]
[15] Physikalisches Institut, Universität Heidelberg, Heidelberg, Germany[a]
[16] Institut für Hochenergiephysik, Universität Heidelberg, Heidelberg, Germany[a]
[17] Institut für Reine und Angewandte Kernphysik, Universität Kiel, Kiel, Germany[a]
[18] Institute of Experimental Physics, Slovak Academy of Sciences, Košice, Slovak Republic[f,j]
[19] School of Physics and Chemistry, University of Lancaster, Lancaster, UK[b]
[20] Department of Physics, University of Liverpool, Liverpool, UK[b]
[21] Queen Mary and Westfield College, London, UK[b]
[22] Physics Department, University of Lund, Lund, Sweden[g]
[23] Physics Department, University of Manchester, Manchester, UK[b]
[24] CPPM, Université d'Aix-Marseille II, IN2P3-CNRS, Marseille, France
[25] Institute for Theoretical and Experimental Physics, Moscow, Russia
[26] Lebedev Physical Institute, Moscow, Russia[f]
[27] Max-Planck-Institut für Physik, München, Germany[a]

2

[28] LAL, Université de Paris-Sud, IN2P3-CNRS, Orsay, France

[29] LPNHE, Ecole Polytechnique, IN2P3-CNRS, Palaiseau, France

[30] LPNHE, Universités Paris VI and VII, IN2P3-CNRS, Paris, France

[31] Institute of Physics, Czech Academy of Sciences of the Czech Republic, Praha, Czech Republic[f,h]

[32] Nuclear Center, Charles University, Praha, Czech Republic[f,h]

[33] INFN Roma 1 and Dipartimento di Fisica, Università Roma 3, Roma, Italy

[34] Paul Scherrer Institut, Villigen, Switzerland

[35] Fachbereich Physik, Bergische Universität Gesamthochschule Wuppertal, Wuppertal, Germany[a]

[36] DESY, Institut für Hochenergiephysik, Zeuthen, Germany[a]

[37] Institut für Teilchenphysik, ETH, Zürich, Switzerland[i]

[38] Physik-Institut der Universität Zürich, Zürich, Switzerland[i]

[39] Institut für Physik, Humboldt-Universität, Berlin, Germany[a]

[40] Rechenzentrum, Bergische Universität Gesamthochschule Wuppertal, Wuppertal, Germany[a]

# 1 Introduction

For a complete understanding of the strong interaction it is necessary not only to survey short range, hard partonic interactions, but also the long range soft interactions that make up the bulk of hadron-hadron and photon-hadron cross sections at high energy. The lack of a hard scale in such soft processes makes calculations within quantum chromodynamic theory (QCD) problematic, and so these processes are usually described using the phenomenology of Regge theory [1] by the $t$-channel exchange of mesons [2] and, at high energy, by the leading vacuum singularity, the pomeron[1] ($\mathbb{P}$) [3]. Measurements of deep-inelastic diffraction, made possible for the first time with the HERA electron-proton ($ep$) collider[2], offer a unique chance to study the soft scattering process with a hard virtual photon probe. It is hoped that precision measurements of diffraction in deep-inelastic scattering (DIS) will guide the formulation of a 'reggeon field theory' that encompasses both hard and soft aspects of the strong force [4,5] and will therefore provide a more complete understanding of QCD.

Following the observation of deep-inelastic scattering events with a rapidity gap [6,7], first measurements were made of the contribution of such events to the DIS cross section, quantified in terms of the differential structure function $F_2^{D(3)}$ [8,9]. These measurements demonstrated that the rapidity gap events could be attributed to an $ep$ process in which the interaction is dominantly diffractive. No substantial $Q^2$ dependence of $F_2^{D(3)}$ was observed, thus indicating that the substructure of diffractive exchange was of a point-like, presumably partonic, nature.

Presented here is a new measurement of $F_2^{D(3)}$, based upon the data collected by H1 during 1994. The measurement is made using data in which a forward rapidity gap is observed so that the hadronic final state is partitioned into two distinct subsystems $X$ and $Y$, where $Y$ is the system with rapidity closest to that of the incident proton. System $X$ is measured with the main components of the H1 detector, whereas system $Y$ is not detected directly but the location of the rapidity gap implies its mass is less than $1.6\,\mathrm{GeV}$. The data amount to a factor $\sim 10$ increase in statistics compared to our previous analysis [8] and they permit a substantially more accurate measurement of $F_2^{D(3)}$ over a wider kinematic range. Further, by utilising data taken with the $ep$ interaction vertex shifted by $\sim 70\,\mathrm{cm}$ along the proton beam direction, the measurement is extended to considerably lower values of $Q^2$ than hitherto possible.

# 2　Cross Section Definition and Kinematic Variables

In the analysis presented in this paper the cross section is defined in terms of a topological decomposition of the final state hadrons. The hadronic final state, defined as all final state particles excluding the scattered electron, is separated into two distinct systems labelled $X$ and $Y$. These are taken to be the two hadronic systems which are separated by the largest interval in rapidity between final state hadrons, where rapidity is calculated in the

---

[1]In this paper the terms 'pomeron exchange' and 'diffraction' are used synonymously.

[2]HERA is able to collide both positrons and electrons with protons. In this paper the term 'electron' is used to describe generically electrons or positrons.

virtual photon-proton centre of mass frame. The system closer in rapidity to that of the incident proton is taken to be the subsystem $Y$. A schematic diagram of an $ep$ scattering, with this decompostion of the final state, is shown in figure 1.

The kinematics of the process can be described by the invariant masses of the two subsystems, $M_X$ and $M_Y$, and the Lorentz scalars

$$x = \frac{-q^2}{2P \cdot q}, \quad y = \frac{P \cdot q}{P \cdot k}, \quad Q^2 = -q^2, \quad t = (P - p_Y)^2. \tag{1}$$

Here $P$ and $k$ are the 4-momenta of the incident proton and electron respectively, $p_Y$ is the 4-momentum of subsystem $Y$ and $q$ is the 4-momentum of the exchanged virtual photon ($\gamma^*$) coupling to the electron. The quantities $x$, $y$ and $Q^2$ are the usual variables used to describe DIS; $t$ is the square of the 4-momentum transferred at the proton-$Y$ vertex. Further useful variables are

$$\beta = \frac{-q^2}{2q \cdot (P - p_Y)} = \frac{Q^2}{Q^2 + M_X^2 - t}, \tag{2}$$

$$\text{and} \quad x_{\mathbb{P}} = \frac{q \cdot (P - p_Y)}{q \cdot P} = \frac{Q^2 + M_X^2 - t}{Q^2 + W^2 - M_p^2} = \frac{x}{\beta}. \tag{3}$$

Here $W^2 = (q + P)^2$ is the square of the centre of mass energy of the virtual photon-proton system and $M_p$ is the proton mass.

The decomposition of the final state has been chosen to most clearly differentiate between various exchange mechanisms. Colourless exchanges can produce states in which $X$ and $Y$ are clearly separated in rapidity and both $M_X$ and $M_Y$ are small compared with $W$. For colour exchange processes, however, the location of the gap is defined by random fluctuations, the average gap size is small and one or both of $M_X$ and $M_Y$ is generally large. In this paper events are selected (see section 4.2) such that $x_{\mathbb{P}} < 0.05$ and $M_Y < 1.6\,\text{GeV}$. This ensures that both $M_X \ll W$ and $M_Y \ll W$, so that $X$ and $Y$ are well separated and the cross section is dominated by colourless exchange processes. In the infinite momentum frame of the incident proton, $x_{\mathbb{P}}$ may be interpreted as the ratio of the momentum carried by the colourless exchange to that of the incident proton, and $\beta$ as the ratio of the momentum carried by the quark coupling to the virtual boson to that of the colourless exchange.

In principle it is possible to measure a differential cross section with events decomposed in the scheme discussed above as a function of five independent variables, and to define a differential structure function $F_2^{D(5)}(x_{\mathbb{P}}, \beta, Q^2, M_Y, t)$

$$\frac{\text{d}^5 \sigma_{ep \to eXY}}{\text{d}x\,\text{d}\beta\,\text{d}Q^2\,\text{d}M_Y\,\text{d}t} = \frac{4\pi\alpha_{em}^2}{\beta^2 Q^4} \left(1 - y + \frac{y^2}{2(1 + R^{D(5)})}\right) F_2^{D(5)}. \tag{4}$$

Here $\alpha_{em}$ is the fine structure constant and $R^{D(5)}(\beta, Q^2, x_{\mathbb{P}}, t, M_Y)$ is the ratio of the longitudinal to the transverse photon cross sections. For the data used in this paper, however, the system $Y$ is not measured directly, so that a differential measurement as a function of $M_Y$ and $t$ is not possible. Instead a measurement of the triple differential cross section $\frac{\text{d}^3 \sigma_{ep \to eXY}}{\text{d}x\,\text{d}\beta\,\text{d}Q^2}$ is made, where an implicit integration is performed over the two

5

unmeasured quantities such that $M_Y < 1.6\,\mathrm{GeV}$ and $|t| < 1\,\mathrm{GeV}^2$. The cross section is chosen to include, and is expected to be dominated by, the single dissociative process $\gamma^* p \to Xp$. The differential structure function $F_2^{D(3)}(x_{\mathbb{P}}, \beta, Q^2)$ is defined and, following the usual convention [8,10,11], is extracted with the assumption of $R^{D(5)} = 0$.

$$\frac{\mathrm{d}^3 \sigma_{ep \to eXY}}{\mathrm{d}x\,\mathrm{d}\beta\,\mathrm{d}Q^2} = \frac{4\pi\alpha_{em}^2}{\beta^2 Q^4}(1 - y + \frac{y^2}{2}) F_2^{D(3)}. \tag{5}$$

The influence of a non-zero value of $R^{D(5)}$ is discussed further in section 5.

# 3    Simulation of Deep-inelastic $ep$ Interactions

In this analysis Monte Carlo simulations are used to correct the data for the effects of losses and smearing. A mixture of several models is used in order to best reproduce the data since no single event generator gives a complete description of all possible DIS final states. Each generated event sample includes a full simulation of the H1 detector and is passed through the same analysis chain as the data.

The RAPGAP generator [12] is used to generate the process $ep \to eXp$ in the kinematic region $M_X > 1.1\,\mathrm{GeV}$ and $x_{\mathbb{P}} < 0.1$. The model has two components in which the proton couples to a pomeron ($\mathbb{P}$) or a meson ($\mathbb{R}$), which subsequently undergoes a hard collision with the incident electron. The pomeron and meson fluxes are taken to follow a simple Regge motivated form [13] with an exponential $t$ dependence so that

$$F_2^{D(4)}(x_{\mathbb{P}}, \beta, Q^2, t) = \frac{e^{B_{\mathbb{P}} t}}{x_{\mathbb{P}}^{2\alpha_{\mathbb{P}}(t)-1}} F_2^{\mathbb{P}}(\beta, Q^2) + \frac{e^{B_{\mathbb{R}} t}}{x_{\mathbb{P}}^{2\alpha_{\mathbb{R}}(t)-1}} F_2^{\mathbb{R}}(\beta, Q^2), \tag{6}$$

where the pomeron and meson trajectories are assumed to have the linear form, $\alpha(t) = \alpha(0) + \alpha' t$. The values for the intercepts $\alpha_{\mathbb{P}}(0) = 1.18$ and $\alpha_{\mathbb{R}}(0) = 0.6$ are chosen such that $F_2^{D(3)}(x_{\mathbb{P}}, \beta, Q^2)$ from the generator is in close agreement with the results of the phenomenological fit presented in section 5. The values for the slope parameters, $B_{\mathbb{P}}$ and $B_{\mathbb{R}}$, and the shrinkage parameters, $\alpha'_{\mathbb{P}}$ and $\alpha'_{\mathbb{R}}$, are not constrained by this analysis. The value assumed for the slope parameter of the pomeron, $B_{\mathbb{P}} = 6\,\mathrm{GeV}^{-2}$, matches the value obtained in a DIS measurement in which the leading proton was detected [14]. Since the shrinkage in the forward peak of the diffractive cross section has not been measured at high $Q^2$ and, since the value used in the generator leads to negligible changes to the measurements presented in this paper, $\alpha'_{\mathbb{P}}$ is set to zero. The assumed values of $B_{\mathbb{R}} = 2\,\mathrm{GeV}^{-2}$ and $\alpha'_{\mathbb{R}} = 0.9\,\mathrm{GeV}^{-2}$ are taken from hadron scattering experiments [15,16].

The pomeron structure function $F_2^{\mathbb{P}}(\beta, Q^2)$ assumed in the generator is derived from parton distributions taken from a QCD fit to the present data similar to that described in section 6. The meson structure function $F_2^{\mathbb{R}}(\beta, Q^2)$ is taken from the GRV parameterisation of the structure function of the pion [17]. The structure functions are assumed to evolve with $Q^2$ according to the leading order DGLAP evolution equations [18]. In addition to the $\mathcal{O}(\alpha_{em})$ quark-parton model diagram ($eq \to eq$), boson-gluon fusion ($eg \to eq\bar{q}$) and QCD-Compton ($eq \to eqg$) processes are generated according to the $\mathcal{O}(\alpha_{em}\alpha_s)$ matrix elements. Higher order QCD corrections are provided either by the colour dipole model

6

as implemented in ARIADNE [19] or parton showers similar to those used in simulations of inclusive DIS (for example see LEPTO [20]). QED radiative processes are included via an interface to the program HERACLES [21].

The low mass region of diffractive production ($M_X < 1.1\,\text{GeV}$) is modelled with the DIFFVM [22] generator, which simulates the production of the vector mesons $\rho(770)$, $\omega(782)$ and $\phi(1020)$. The cross sections are taken from measurements for $\rho(770)$ and $\phi(1020)$ production in DIS [23–26] and a ratio of $\omega(782) : \rho(770)$ of $1 : 9$ as given by quark counting rules. The $Q^2$ and $W$ dependences of the cross sections are assumed to follow those measured for $\rho(770)$ production [23].

The DIFFVM generator is also used to model proton dissociation. The cross section for proton dissociation is assumed to have a $\mathrm{d}\sigma/\mathrm{d}M_Y \propto 1/M_Y^2$ dependence at large $M_Y$, with a parameterisation based on measurements of proton dissociation on deuterium [27] for the low mass region. Two different decay mechanisms are considered: decay with limited $p_T$ following the Lund fragmentation scheme [28], or isotropic phase space decay with multiplicity following KNO scaling laws [29]. The ratio of proton dissociation to elastic proton interactions is assumed to be 1.

The kinematic region of high $M_Y$ or high $x_{\mathbb{P}}$ ($M_Y > 5\,\text{GeV}$ or $x_{\mathbb{P}} > 0.1$) is modelled with DJANGO [30]. This model is a deep-inelastic $ep$ generator based on the QCD substructure of the proton, with a colour string between the proton remnant and the current fragmentation region. Higher order QCD corrections are provided by the colour dipole model and QED radiative effects are implemented via an interface to HERACLES. DJANGO has been shown to reproduce well many aspects of the DIS final state including measurements of energy flows in the forward region [31]. The normalisation for DJANGO was chosen such that the sum of the cross sections from RAPGAP, DIFFVM and DJANGO is in approximate agreement with that corresponding to the measured proton structure function $F_2(x, Q^2)$ [32].

The PHOJET [33] generator was used to estimate background from photoproduction events. In PHOJET events are generated as five distinct subprocesses: non-diffraction, elastic vector meson production, vector meson production with proton dissociation, single photon diffraction dissociation and double diffraction dissociation. These subprocesses are mixed such that the total photoproduction cross section and the subprocess ratios are in agreement with measurements made at HERA [34].

Background events arising from the QED Compton process ($ep \rightarrow ep\gamma$) were simulated using the COMPOS generator [35].

# 4    Experimental Technique

The data presented here were obtained by H1 in 1994, when HERA was colliding $27.5\,\text{GeV}$ positrons with protons at $820\,\text{GeV}$. The results shown are based on an integrated luminosity of $1.96\,\text{pb}^{-1}$ with the interaction point in its usual position relative to H1. A further $0.06\,\text{pb}^{-1}$ of data, taken with the interaction point shifted by $70\,\text{cm}$ in the proton direction, are also used. These data enable measurements to be made at lower values of $Q^2$. The two event samples are referred to as the nominal vertex and shifted vertex data respectively.

## 4.1 H1 Apparatus

The H1 detector is a composite, multi-purpose apparatus, designed to investigate the final states of high energy electron-proton interactions. Given here is only a brief outline of the components of the H1 detector of relevance to the present analysis; for a more detailed technical description see [36]. A right handed co-ordinate system is employed at H1 that has its $z$-axis pointing in the proton beam, or forward, direction.

Surrounding the interaction point are the central and forward tracking detectors. These are situated in a uniform 1.15 T magnetic field, enabling momentum measurement of charged particles over the pseudorapidity range $-1.5 < \eta < 2.8$.[3] A multi-wire proportional chamber (BPC) gives additional acceptance for charged particles in the backward region $(-3.0 < \eta < -1.5)$. Surrounding the track detectors in the forward and central directions $(-1.5 < \eta < 3.7)$ is a fine grained liquid argon calorimeter (LAr) and in the backward region $(-3.5 < \eta < -1.5)$ is a lead-scintillator electromagnetic calorimeter (BEMC). The main calorimeters are surrounded by an instrumented iron backing calorimeter.

Components of the H1 detector positioned forward of the LAr are used in this analysis to tag particles at high values of pseudorapidity. These 'forward detectors' are sensitive to the secondaries produced by the rescattering of primary particles with the beam pipe and adjacent material, and are thus sensitive to larger pseudorapidities than would be expected on the basis of their geometrical acceptance alone. A copper-silicon plug calorimeter (PLUG) allows energy measurements to be made over the range $3.5 < \eta < 5.5$. Three double layers of drift chambers of the forward muon detector (FMD) are sensitive to particles produced at higher pseudorapidities $5.0 < \eta < 6.5$. The proton remnant tagger (PRT), consisting of seven double layers of scintillators, covers the region $6.0 < \eta < 7.5$.

Two electromagnetic calorimeters (LUMI) situated downstream in the electron beam direction measure electrons and photons from the bremsstrahlung process $ep \to ep\gamma$ for the purpose of luminosity determination.

## 4.2 Event Selection

Deep-inelastic scattering events are selected by requiring a compact energy deposit of at least 10.5 GeV in the BEMC and a BPC hit associated with this cluster. Background in the DIS sample is suppressed by requiring a vertex reconstructed by the track detectors within 30 cm of the mean $z$ position of the vertex, a minimum $Q^2$ and at least two reconstructed non-associated objects (tracks or clusters) besides the scattered electron in the final state. Further cuts, requiring an agreement between different kinematic reconstruction methods, are introduced to reduce radiative corrections. The precise cuts employed are summarised in table 1a. A more extensive discussion of the DIS event selection at H1 may be found in [32].

A subsample of events is selected where colourless exchange processes (such as diffraction) are expected to dominate. This is achieved by requiring no activity above noise levels in any of the forward detectors or in the most forward part of the LAr (see table 1b

---

[3]The pseudorapidity $(\eta = -\ln \tan \theta/2)$ coverage of each detector component is given for the vertex in its nominal position.

8

a)

| (1) | $E'_e > 10.5\,\mathrm{GeV}$ |
|---|---|
| (2) | $Q^2 > 8.0\;(3.5)\,\mathrm{GeV}^2$ |
| (3) | $156°(163°) < \theta_e < 174°(176°)$ |
| (4) | $\varepsilon_1 < 5\,\mathrm{cm}$ |
| (5) | $\varepsilon_2 < 5\,\mathrm{cm}$ |
| (6) | $|z_{\mathrm{vtx}} - \bar{z}_{\mathrm{vtx}}| < 30\,\mathrm{cm}$ |
| (7) | $N_{\mathrm{track}} + N_{\mathrm{cluster}} > 1$ |
| (8) | $-0.55 < y_h - y_e < 0.25$ |
| (9) | $|y_{DA} - y_e| < 0.2(0.3)$ |

b)

| (10) | $\eta_{\max}^{\mathrm{LAr}} < 3.3$ |
|---|---|
| (11) | $E_{\mathrm{PLUG}} < 5\,\mathrm{GeV}$ |
| (12) | $N_{\mathrm{FMD}} < 2$ |
| (13) | $N_{\mathrm{PRT}} = 0$ |

**Table 1:** Summary of event selection criteria for a) inclusive DIS events and b) additional cuts to select large rapidity gap events. The shifted vertex cuts are given in brackets where they are different from the nominal vertex cuts. Section 4.3 gives details of the methods used to reconstruct the DIS kinematic variables. Cuts 1–3 ensure the scattered electron is within the acceptance region of the BPC and BEMC; cuts 4 and 5 are electron identification estimators, $\varepsilon_1$ is the electron cluster radius, $\varepsilon_2$ is the distance from the closest hit in the BPC to the centroid of the electron cluster [32]; cuts 6 and 7 require there to be at least 2 reconstructed objects in the hadronic final state of which one must be a track pointing to the interaction region; cuts 8 and 9 ensure agreement between different kinematic reconstruction techniques; cut 10 requires that there is no activity observed in LAr above noise levels for $\eta > 3.3$; cuts 11–13 ensure that there is no activity above noise levels in the forward detectors [37].

for details of the cuts). The selection implies that systems $X$ and $Y$ (as defined in section 2) are well separated, such that $X$ is fully contained in the main detector components and $Y$ passes unobserved into the forward beam pipe. The maximum allowed value of pseudorapidity for particles from the system $X$ of 3.3 (cut (10) in table 1b) ensures that $x_{\mathrm{I\!P}} \lesssim 0.05$. The fact that no part of the system $Y$ is detected in the forward detectors restricts $M_Y \lesssim 1.6\,\mathrm{GeV}$ and $|t| \lesssim 1\,\mathrm{GeV}^2$. This sample of events is referred to hereafter as the 'large rapidity gap' event sample. The number of selected events is 13956 in the nominal vertex sample and 760 in the shifted vertex sample.

The only backgrounds in the large rapidity gap event sample that were found to be significant were from photoproduction and the QED Compton process $ep \to ep\gamma$. Photoproduction background arises when the scattered electron escapes undetected along the beam pipe and a final state hadron fakes a BEMC electron cluster. This background was estimated using the PHOJET simulation and is found to contribute most significantly at high $y$ and low $Q^2$. The overall photoproduction background was estimated to be 0.3 % of the large rapidity gap event sample and at most 13 % for any single data bin.

QED Compton events were studied with the COMPOS generator and found to be effectively suppressed by cut (7) in table 1. Residual QED Compton background arises when the final state photon converts in material in front of the BEMC, producing a BPC hit and is mistaken for the scattered electron. The true electron and some residual calorimeter noise fake the hadronic final state. This background was found to contribute most significantly at high $\beta$ and high $y$. The overall QED Compton background is estimated to be 0.6 % of the large rapidity gap event sample and contributes a maximum of

9

15 % in any single bin.

Each background source was subtracted bin by bin.

## 4.3  Reconstruction of the Kinematic Variables

The kinematic variables, defined in section 2, are calculated from the energy and the polar angle of the scattered electron ($E'_e$, $\theta_e$) and from the 4-vector of the hadronic final state ($E_h$, $p_{xh}$, $p_{yh}$, $p_{zh}$). $E'_e$ is reconstructed from the cluster with the largest energy in the BEMC passing the cuts described in table 1, and $\theta_e$ is the angle defined by the $z$-vertex and the BPC hit associated with the electron. The hadronic 4-vector is reconstructed by combining information from the track detectors and calorimeters using an energy flow algorithm, which improves the resolution compared to methods relying on single detector components [38].

A key feature of the H1 experiment is its ability to measure both the electron and hadronic final state well, thus providing a number of methods for reconstructing the kinematic variables. In this analysis the kinematics are reconstructed using a method that combines the electron method, in which the kinematics are reconstructed solely from the scattered electron, and the double angle method, which uses only angles of the hadronic final state and the scattered electron [39]. The two methods are combined in order to utilise the optimal resolution of the electron method at high $y$ and the double angle method at low $y$. We reconstruct $y$ as

$$y = y_e^2 + y_{DA}(1 - y_{DA}),\tag{7}$$

$$\text{where}\quad y_e = 1 - \frac{E'_e}{E_e}\sin^2(\theta_e/2)\quad\text{and}\quad y_{DA} = \frac{\sin\gamma(1 + \cos\theta_e)}{\sin\gamma + \sin\theta_e + \sin(\theta_e + \gamma)},\tag{8}$$

$$\text{with}\quad \cos\gamma = \frac{p_{xh}^2 + p_{yh}^2 - (E_h - p_{zh})^2}{p_{xh}^2 + p_{yh}^2 + (E_h - p_{zh})^2},\tag{9}$$

and $E_e$ is the electron beam energy. As demonstrated by figure 2(a), this '$y$ weighted averaging method' provides excellent resolution in $y$ over its full range. $Q^2$ is reconstructed from $y$ and the angle of the scattered electron

$$Q^2 = \frac{4E_e^2(1 - y)}{\tan^2(\theta_e/2)}.\tag{10}$$

Two additional kinematic reconstruction methods are used to reconstruct $y$ and/or $Q^2$ for the purposes of cross checks and event selection cuts. These are the hadron method [40] for which $y_h = (E_h - p_{zh})/(2E_e)$ and the $\Sigma$ method [41] for which $y_\Sigma = y_h/(1 + y_h - y_e)$ and $Q_\Sigma^2 = 4E_e'^2\sin^2(\theta_e)/(1 - y_\Sigma)$. The Bjorken scaling variable $x$ is calculated in all methods as $Q^2/sy$ where $s$ is the $ep$ centre of mass energy.

For the large rapidity gap event sample the system $X$ is fully contained within the main detector, so that the visible hadronic final state corresponds to the system $X$. It is thus possible to reconstruct the variables $M_X$, $\beta$ and $x_{\mathbb{P}}$ well. The invariant mass $M_X$ is reconstructed with a method that utilises the optimised reconstruction of $y$

$$M_X^2 = (E_h^2 - p_{xh}^2 - p_{yh}^2 - p_{zh}^2)\frac{y}{y_h}.\tag{11}$$

10

A constant scale factor of 1.10, determined from the simulations, is applied to the reconstructed $M_X$ to correct for residual losses, mainly due to dead material in front of the calorimeters. As demonstrated in figure 2(b), the resulting $M_X$ is well reconstructed across the kinematic range of the measurement with a resolution of about 25 %. The other kinematic quantities are determined using equations (2) and (3), with the approximation $|t| \ll M_X^2 + Q^2$.

The accuracy of the reconstruction method and the ability of the simulation to describe the data were checked in a variety of ways. Figure 3(a) shows the ratio of the transverse momentum of the visible hadrons to that of the electron, which for a perfect detector should have a narrow width and peak at 1. At the detector level it can be seen that the peak is smeared with $\sigma \approx 30\%$, but with a mean close to 1, showing that there are no substantial losses of final state hadrons. Figure 3(b) shows that there is good agreement between $y$ when reconstructed using the electron or double angle methods before combination. For both these distributions the simulation is in good agreement with the data, showing that the resolutions and biases of the detector are well understood.

Since an understanding of bin migrations depends not only on the resolution in the kinematic quantities, but also on the form of the differential cross section, it is important that the cross section used as the input to the simulations closely matches that of the data. Figures 3(c) and 3(d), which show the reconstructed $\beta$ and $\theta_e$ spectra, give an indication that this is indeed the case. Similar agreement is found for the $x_{\mathbb{P}}$, $M_X$ and $y$ spectra.

## 4.4 Evaluation of the Differential Structure Function

The large rapidity gap event sample is used to measure the differential cross section $\frac{d^3\sigma}{dx\,d\beta\,dQ^2}$ for the process $ep \to eXY$ as defined in section 2 for $4.5 < Q^2 < 75\,\mathrm{GeV}^2$, $0.0002 < x_{\mathbb{P}} < 0.04$ and $0.04 < \beta < 0.9$. The data are divided into three-dimensional bins in $x$, $\beta$ and $Q^2$. The Monte Carlo models are used to correct bin by bin for losses, smearing and backgrounds. No difference was observed within the statistical errors of the simulations between the acceptances when evaluated using the ARIADNE or parton showers fragmentation options within RAPGAP. The average of the two acceptances was therefore taken. An additional overall correction of $1.11 \pm 0.05$ is applied to account for events lost due to noise in the forward detectors, which is not simulated in the Monte Carlo models. This correction is evaluated from randomly triggered events, in which there is no requirement of particle activity in the detector. Radiative corrections are applied bin by bin using the HERACLES interface to RAPGAP.

Since the cross section is expected to vary smoothly with the kinematic variables for bins that lie away from the resonance region of the light vector mesons ($\rho^0$, $\omega$, $\phi$, $\rho'$), the cross section is corrected to that at the bin centre ($x_c$, $\beta_c$, $Q_c^2$) for bins where $M_{Xc} > 2\,\mathrm{GeV}$. For these bins the main deviation from a smooth variation of the cross section is expected to arise from elastic $J/\psi$ and $\psi(2S)$ production, which contribute a maximum to any single bin of approximately 5% and 1% respectively [23,42]. These contributions are not subtracted but a systematic error equal to the expected magnitude of the contribution is added to the systematic error. For the bins that have a mass interval such that they cover one or more of the light vector mesons ($M_{Xc} < 2\,\mathrm{GeV}$), the dependence of the cross section

11

on $x$ and $Q^2$ is expected to be smooth, but there are likely to be substantial deviations from a smooth dependence of the cross section as a function of $\beta$. For this reason the cross section is corrected to the bin centre only in $(x_c, Q^2_c)$ and in $\beta$ it corresponds to the average over the range covered by the bin.

For all selected bins the acceptance is required to be above 0.4, and the purity (i.e. the fraction of the number of events both generated and reconstructed in a bin to the number reconstructed in the bin) is required to be greater than 0.2. The chosen bins have an average acceptance of 0.82 and an average purity of 0.45. The two data samples are combined by taking the shifted vertex data where there is no nominal vertex coverage ($Q^2 < 9\,\mathrm{GeV}^2$) and the nominal vertex data elsewhere ($Q^2 \geq 9\,\mathrm{GeV}^2$).

The statistical errors are formed by adding in quadrature the contribution from the data and that due to the finite statistics of the Monte Carlo simulations. Systematic errors arise from the following sources:

- The error due to uncertainties in the reconstruction of the scattered electron, estimated by changing the electromagnetic energy scale of the BEMC by $\pm 1\%$ and shifting the electron polar angle by $\pm 1$ mrad.

- Uncertainties in the reconstruction of the hadronic final state, estimated by changing the hadronic energy scale of LAr by $\pm 5\%$, that of the BEMC by $\pm 20\%$ and by shifting the energy fraction carried by the tracks by $\pm 3\%$.

- Errors due to our *a priori* ignorance of the input structure function as used in the simulations, estimated by reweighting the generated events by factors $x_{\mathbb{P}}^{\pm 0.2}$ and $(1 \pm 0.3\beta)$. These factors are chosen such that resulting generated structure function is changed by an amount larger than the final errors on the data points. An additional error is assigned to account for smearing of events from kinematic regions where the differential structure function is not measured. This error is conservatively estimated by changing the number of events generated with $x_{\mathbb{P}} > 0.1$ and/or $M_Y > 5\,\mathrm{GeV}$ by $\pm 50\%$.

- Errors due to the uncertainty in the $t$ dependence, estimated by reweighting by $e^{\pm 2t}$.

- The uncertainty in the correction due to smearing of events across the boundary $M_Y = 1.6\,\mathrm{GeV}$, estimated by changing the PLUG energy scale by $\pm 30\%$, by changing the PRT efficiency by $\pm 20\%$, by taking the difference between the correction evaluated using isotropic and limited $p_T$ proton dissociation models and by varying the ratio of double dissociation to single photon dissociation assumed in the simulation between 0.5 and 2.0, such that the range covers that measured in various proton dissociation processes in DIS and photoproduction [26, 38, 43].

- The uncertainty in the number of background events, estimated as $50\%$ of the photoproduction and $30\%$ of the QED Compton background.

- The uncertainty in the bin centre correction due to contributions from high mass resonances, estimated by assuming an error of $5\%$ for all bins which contain the $J/\psi$ and $1\%$ for all other bins to account for the $\psi(2S)$ and other possible contributions.

12

- An error of 2% per point is assumed to account for any detector inefficiencies not included in the simulations [32].

- An overall normalisation uncertainty of 4.8% for the nominal vertex data and 6.0% for shifted vertex data, evaluated by adding in quadrature a 4.5% error on the uncertainty due to the correction for events lost due to forward detector noise and the errors on the integrated luminosity of 1.5% and 3.9% for nominal and shifted vertex data.

To check the stability of the results, the analysis was repeated by widely varying the experimental cuts and by changing kinematic reconstruction techniques. Figure 4(a) shows that there is reasonable agreement between the results obtained from the nominal and shifted vertex data samples for the standard analysis in the region of overlap. In figure 4(b) it can be seen that the results do not change significantly if the $\Sigma$ method is used to reconstruct the kinematics. Figures 4(c), (d) and (e) demonstrate that changing the rapidity gap requirement does not greatly change the results. In figures 4(f) it can be seen that even without the requirement of a rapidity gap, when the measurement is made solely on the basis of the reconstructed $M_X$ values in the inclusive data sample, the results obtained are well within the quoted systematic uncertainty.

The measured values of $F_2^{D(3)}(x_{\mathbb{P}}, \beta, Q^2)$, evaluated using equation (5), are listed in table 3 and are also available from [44].

The quantity $x_{\mathbb{P}} F_2^{D(3)}(x_{\mathbb{P}}, \beta, Q^2)$ is shown[4] in figure 5 as a function of $x_{\mathbb{P}}$ for different $\beta$ and $Q^2$ values. It can be seen that over most of the kinematic region covered $x_{\mathbb{P}} F_2^{D(3)}(x_{\mathbb{P}}, \beta, Q^2)$ is either falling, or approximately constant, as function of increasing $x_{\mathbb{P}}$. Qualitatively this is consistent with our earlier observation [8] of a dominant diffractive contribution with an intercept $\alpha_{\mathbb{P}}(0) \gtrsim 1$. However, the more precise data of the present analysis show that there is a clear change in the $x_{\mathbb{P}}$ dependence at low $\beta$ where there is a tendency for it to increase at the highest $x_{\mathbb{P}}$. A quantitative study of this $x_{\mathbb{P}}$ behaviour is given in terms of Regge amplitudes in the following section.

# 5 Regge Parameterisation of the Data

An appropriate phenomenological framework to study the behaviour of the DIS colour singlet exchange cross section is provided by Regge theory [1,2]. This theory has proved to be remarkably successful in describing high energy hadron-hadron and hadron-photon cross sections (see for example [13,15,38,45]) as well as early measurements of $F_2^{D(3)}$ [8,9, 14]. Regge theory in its simple form[5], when applied to deep-inelastic scattering, provides information on the $x_{\mathbb{P}}$ dependence at fixed $\beta$, $Q^2$ and $t$. Since there is much theoretical uncertainty concerning the precise form of the Regge model which is appropriate for colour singlet exchange in DIS, several fits to the data are performed with different assumptions. In all fits the $\chi^2$ values are quoted for statistical errors only.

---

[4] $x_{\mathbb{P}} F_2^{D(3)}(x_{\mathbb{P}}, \beta, Q^2)$ is plotted, rather than $F_2^{D(3)}(x_{\mathbb{P}}, \beta, Q^2)$, in order to show more clearly any deviations of the data from a simple power law behaviour on $x_{\mathbb{P}}$.

[5] No attempt has been made in this paper to describe $F_2^{D(3)}(x_{\mathbb{P}}, \beta, Q^2)$ using 'triple-Regge' theory, which would provide an additional prediction for the dependence of the cross section on $\beta$.

For fit A it is assumed that $F_2^{D(3)}$ may be factored into a pomeron flux and pomeron structure function [11]

$$F_2^{D(3)}(x_{\mathbb{P}}, \beta, Q^2) = f_{\mathbb{P}/p}(x_{\mathbb{P}})F_2^{\mathbb{P}}(\beta, Q^2). \tag{12}$$

The pomeron flux is taken to follow a Regge behaviour with a peripheral $t$ dependence and a linear trajectory $\alpha_{\mathbb{P}}(t) = \alpha_{\mathbb{P}}(0) + \alpha'_{\mathbb{P}} t$ such that

$$f_{\mathbb{P}/p}(x_{\mathbb{P}}) = \int_{t_{cut}}^{t_{min}} \frac{e^{B_{\mathbb{P}} t}}{x_{\mathbb{P}}^{2\alpha_{\mathbb{P}}(t)-1}} \mathrm{d}t, \tag{13}$$

where $|t_{min}|$ is the minimum kinematically allowed value of $|t|$ and $t_{cut} = -1\,\mathrm{GeV}^2$ is the limit of the measurement. The values for $B_{\mathbb{P}}$ and $\alpha'_{\mathbb{P}}$ cannot be constrained in the fit and are assumed to be the same as those obtained from analyses of hadron-hadron data. These values give consistent results with a measurement of the $t$ dependence of the colour singlet exchange cross section averaged over the other kinematic quantities [14]. Table 2 lists the assumed values for all fixed parameters used in this and subsequent fits. The value of $\alpha_{\mathbb{P}}(0)$ is left as a free parameter in the fit as is $F_2^{\mathbb{P}}(\beta, Q^2)$ at each $(\beta, Q^2)$ where there are data. A complication arises from the lack of knowledge of $R^{D(5)}(\beta, Q^2, x_{\mathbb{P}}, t, M_Y)$, the ratio of the longitudinal to the transverse cross section. The effect of a non-zero value for $R^{D(5)}$ produces a decrease in the $F_2^{D(3)}$ extracted at large $y$ relative to that obtained with the assumption $R^{D(5)} = 0$. The maximum value of $y$ for any of the H1 data is at $y = 0.55$ which leads to a maximum shift in $F_2^{D(3)}$ of 34% if $R^{D(5)} = \infty$. Since these shifts are large compared with the errors on the data points only those data with $y < 0.45$ are fitted thus limiting the shift to a maximum of 18%. The difference when $R^{D(5)} = \infty$ instead of $R^{D(5)} = 0$ is included as part of the 'model dependence' error for all fits.

| Quantity | Value | | Source |
|---|---|---|---|
| $R^{D(5)}$ | 0 | $^{+\infty}_{-0}$ | |
| $\alpha'_{\mathbb{P}}$ | 0.26 | $\pm 0.26\ \mathrm{GeV}^{-2}$ | [46] |
| $\alpha'_{\mathbb{R}}$ | 0.90 | $\pm 0.10\ \mathrm{GeV}^{-2}$ | [16] |
| $B_{\mathbb{P}}$ | 4.6 | $^{+3.4}_{-2.6}\ \mathrm{GeV}^{-2}$ | [46] |
| $B_{\mathbb{R}}$ | 2.0 | $\pm 2.0\ \mathrm{GeV}^{-2}$ | [15] |

**Table 2:** Values assumed for the fixed parameters in the Regge fits and the sources from which they are taken. Each quantity is defined in the text. Contributions to the model dependence errors are formed by repeating the fits after separately varying each parameter by the quoted uncertainties.

Fit A yields a rather poor $\chi^2/\mathrm{ndf}$ of 257.8/168. Changing the form of the $x_{\mathbb{P}}$ dependence or the values of the fixed parameters of the fit, whilst still retaining the factorisation hypothesis, cannot explain the data simultaneously at both high and low $\beta$. The exchange of a single factorisable Regge trajectory in the $t$-channel does not, therefore, provide an acceptable description of the dependence of $F_2^{D(3)}$ on $x_{\mathbb{P}}$.

A natural explanation of the observed factorisation breaking is the presence of a sub-leading exchange in addition to the leading pomeron. Such an exchange is necessary to describe the energy dependence of total, elastic and dissociative photoproduction and hadron-hadron cross sections [15,38,47].

14

In fits B and C we assume a subleading exchange, made up from the set of reggeons which lie on the approximately degenerate trajectory $\alpha_{\mathbb{IR}}(t) \simeq 0.55 + 0.9t$ and which carry the quantum numbers of the $\rho$, $\omega$, $a$ or $f$ meson. It is assumed that each of these exchanges can be expressed as the product of a flux and a meson structure function akin to equation (12) and that the structure function of each exchange is the same. The situation is complicated by the possibility of interference between the terms which describe the pomeron and the $f$ meson trajectory[6] so that $F_2^{D(3)}$ takes the form

$$F_2^{D(3)}(x_{\mathbb{IP}}, \beta, Q^2) = f_{\mathbb{IP}/p}(x_{\mathbb{IP}}) F_2^{\mathbb{IP}}(\beta, Q^2) + f_{\mathbb{IR}/p}(x_{\mathbb{IP}}) F_2^{\mathbb{IR}}(\beta, Q^2)$$
$$+ 2 I f^I(x_{\mathbb{IP}}) \sqrt{F_2^{\mathbb{IP}}(\beta, Q^2) F_2^{\mathbb{IR}}(\beta, Q^2)}, \tag{14}$$

with

$$f_{\mathbb{IR}/p}(x_{\mathbb{IP}}) = \int_{t_{cut}}^{t_{min}} \frac{e^{B_{\mathbb{IR}} t}}{x_{\mathbb{IP}}^{2\alpha_{\mathbb{IR}}(t) - 1}} \, \mathrm{d}t. \tag{15}$$

The interference flux is derived from the pomeron and meson fluxes with the phase completely specified by the signature factors of the pomeron and the $f$ [13] in the form of

$$f^I(x_{\mathbb{IP}}) = \int_{t_{cut}}^{t_{min}} \cos\left(\frac{\pi}{2}[\alpha_{\mathbb{IP}}(t) - \alpha_{\mathbb{IR}}(t)]\right) \frac{e^{(B_{\mathbb{IP}} + B_{\mathbb{IR}}) t/2}}{x_{\mathbb{IP}}^{\alpha_{\mathbb{IP}}(t) + \alpha_{\mathbb{IR}}(t) - 1}} \mathrm{d}t. \tag{16}$$

The quantity $I$ denotes the degree of coherence and is assumed to take any value from 0, when no $f$ contributes to the subleading exchange, and up to 1 for $f$ dominance of the subleading reggeon [38]. In these fits $I$ is assumed independent of $\beta$ and $Q^2$. The quantities $\alpha_{\mathbb{IP}}$, $\alpha_{\mathbb{IR}}$, $F_2^{\mathbb{IP}}(\beta, Q^2)$ and $F_2^{\mathbb{IR}}(\beta, Q^2)$ are left as free fit parameters and a constraint that $F_2^{\mathbb{IR}}(\beta, Q^2) \geq 0$ is imposed.

For fit B no interference is assumed by setting $I = 0$. The fit gives an acceptable $\chi^2/\mathrm{ndf}$ of 120.7/121 and describes the deviations from factorisation of $F_2^{D(3)}$ well. Values of $\alpha_{\mathbb{IP}}(0) = 1.200 \pm 0.017(\mathrm{stat.}) \pm 0.011(\mathrm{sys.})^{+0.029}_{-0.034}(\mathrm{model})$ and $\alpha_{\mathbb{IR}}(0) = 0.57 \pm 0.14(\mathrm{stat.}) \pm 0.11(\mathrm{sys.})^{+0.03}_{-0.07}(\mathrm{model})$ are obtained. The systematic errors on both extracted quantities are estimated by adding in quadrature the differences obtained from the central fit value after imposing each of the variations described in section 4.4. The model dependence error is estimated in a similar manner by varying the values of the fixed parameters of the fit over the ranges listed in table 2. These ranges represent our best estimate of the likely variation in the present data after examining the spread in the values obtained in other scattering processes.

In fit C maximal interference is assumed between the pomeron and the meson trajectory ($I = 1$). A very similar $\chi^2/\mathrm{ndf}$ of 120.4/121 is obtained, with a similar value of $\alpha_{\mathbb{IP}}(0) = 1.206 \pm 0.022(\mathrm{stat.}) \pm 0.013(\mathrm{sys.})^{+0.030}_{-0.035}(\mathrm{model})$ and a lower value of $\alpha_{\mathbb{IR}}(0) = 0.44 \pm 0.08(\mathrm{stat.}) \pm 0.07(\mathrm{sys.})^{+0.06}_{-0.05}(\mathrm{model})$. The results of this fit are shown in figure 5. It can be seen that at constant $x_{\mathbb{IP}}$ the meson component and the interference part fall much more steeply as $\beta$ increases than does the pomeron component.

Since fits B and C both give a good description of the data and have similar $\chi^2/\mathrm{ndf}$ it is not possible to determine, with the present data, whether or not interference plays

---

[6]Interference between the pomeron and any of the other subleading mesons trajectories is forbidden by C- and G-parity conservation.

a significant role in DIS colour singlet exchange cross sections. Further precision measurements at high values of $x_{\mathbb{P}}$ are needed to clarify this matter. The results of the two fits do, however, yield compatible results for the intercepts of the pomeron and meson exchanges, and, since it is likely that the truth lies somewhere between the solutions with $I = 0$ and $I = 1$, a best estimate for the values of the intercepts is obtained by averaging the two results and including the difference between the two fits in the model dependent error. This procedure yields

$$\alpha_{\mathbb{P}}(0) = 1.203 \pm 0.020 \text{ (stat.)} \pm 0.013 \text{ (sys.)}^{+0.030}_{-0.035} \text{ (model)}$$
$$\alpha_{\mathbb{R}}(0) = 0.50 \pm 0.11 \text{ (stat.)} \pm 0.11 \text{ (sys.)}^{+0.09}_{-0.10} \text{ (model)}.$$

The value of $\alpha_{\mathbb{P}}(0)$ found in this analysis is significantly larger than that obtained from analyses of soft hadronic cross sections [47,48]. It also exceeds the value $\alpha_{\mathbb{P}}(0) = 1.068 \pm 0.016\text{(stat.)} \pm 0.022\text{(sys.)} \pm 0.041\text{(model)}$, which was obtained from an H1 analysis of the photon diffractive dissociation cross section at $Q^2 = 0$ [38]. The value of $\alpha_{\mathbb{R}}(0)$ agrees with the value of $\simeq 0.55$ obtained in an analysis of total hadronic cross sections [47].

An attempt is made to see if there are any further deviations from factorisation of the pomeron flux within the two-reggeon model described by equation (14). Two separate fits are performed that follow B, but now $\alpha_{\mathbb{P}}(0)$ is allowed to vary as a function of either $\beta$ or $Q^2$ so that $\alpha_{\mathbb{P}}(0) = a_1 + a_2(\beta - 0.5)$ or $\alpha_{\mathbb{P}}(0) = a_1' + a_2' \log_{10}(Q^2/10\text{GeV}^2)$. Both give acceptable $\chi^2/\text{ndf}$ of 120.5/120 and 120.7/120 respectively, but within the errors both fits show that the data are compatible with no change in $\alpha_{\mathbb{P}}(0)$ with $\beta$ or $Q^2$: $a_2 = 0.03 \pm 0.10\text{(stat.)} \pm 0.04\text{(sys.)}^{+0.01}_{-0.06}\text{(model)}$ , $a_2' = 0.004 \pm 0.071\text{(stat.)} \pm 0.014\text{(sys.)}^{+0.003}_{-0.003}\text{(model)}$. Similar results are obtained for fits performed with full interference.

We conclude that the data may be described using a Regge model with two components in which a pomeron contributes along with a subleading exchange. In this two reggeon scenario there is, within experimental errors, no evidence for a change in the pomeron intercept with $\beta$ or $Q^2$ over the kinematic region of this measurement.

# 6 Deep-inelastic Structure of Diffractive Exchange

## 6.1 QCD Extension of the Phenomenological Model

In the universal factorisation hypothesis discussed in section 5, the structure functions $F_2^{\mathbb{P}}(\beta, Q^2)$ and $F_2^{\mathbb{R}}(\beta, Q^2)$ describe the deep-inelastic structure of the pomeron and meson exchanges respectively. It has been suggested that the $Q^2$ evolution of these structure functions may be understood in terms of parton dynamics and therefore perturbative QCD [11,49,50].

To establish whether the data are consistent with such a hypothesis, the phenomenological model presented in section 5 is further developed by assigning parton distribution functions to the pomeron and to the meson. Currently, there is no clear theoretical consensus on how colour singlet exchange processes may be understood within the context of QCD, perturbative or otherwise [51]. Therefore, a simple prescription is adopted in which the parton distributions of both the pomeron and the meson are parameterised in terms of non-perturbative input distributions at some low scale $Q_0^2$. The parton distributions

of the pomeron and of the meson are evolved separately with increasing $Q^2$ according to the DGLAP [18] evolution equations.

For the pomeron, a quark flavour singlet distribution ($z\mathcal{F}_q(z,Q^2) = u+\bar{u}+d+\bar{d}+s+\bar{s}$) and a gluon distribution ($z\mathcal{F}_g(z,Q^2)$) are parameterised in terms of the coefficients $C_j^i$ at a starting scale of $Q_0^2 = 3\,\mathrm{GeV}^2$ such that

$$z\mathcal{F}_i(z,Q^2 = Q_0^2) = \left[\sum_{j=1}^{n} C_j^i \cdot P_j(2z-1)\right]^2 \cdot e^{\frac{a}{z-1}} \tag{17}$$

where $z = x_{i/\mathbb{P}}$ is the fractional momentum of the pomeron carried by the struck parton. If the photon couples directly to a quark ($i = q$) then $z = \beta$, whilst if the photon interacts with a gluon ($i = g$) then $z$ is the fractional momentum carried by the gluon and $0 < \beta < z$. $P_j(\zeta)$ is the $j^{th}$ member in a set of Chebyshev polynomials, which are chosen such that $P_1 = 1$, $P_2 = \zeta$ and $P_{j+1}(\zeta) = 2\zeta P_j(\zeta) - P_{j-1}(\zeta)$. A sum of $n$ orthonormal polynomials is used so that the input distributions are free to adopt the widest possible range of forms for a given number of parameters. Any bias towards a particular solution due to the choice of the functional form of the input distribution is therefore minimised, and the number of terms included in the parameterisation may be matched to the significance of the data. The series is squared to ensure a positive definite parameterisation for all values of $z$ and $C_j^i$.

For the evolution equations to be solvable, the parton distribution functions must tend to zero as $z \to 1$. This is achieved by introducing the exponential term with a positive value of the parameter $a$. Unless otherwise indicated, in the following fits $a$ is set to 0.01 such that this term only influences the parameterisation in the region $z > 0.9$.

The functions $z\mathcal{F}_i(z,Q^2)$ are evolved to higher $Q^2$ using the next-to-leading order DGLAP evolution equations and the contribution to $F_2^{\mathbb{P}}(\beta,Q^2)$ from charm quarks is calculated in the fixed flavour scheme using the photon-gluon fusion prescription given in [52]. The contribution from heavier quarks is neglected.

In the Regge model phenomenological fits B and C described in section 5 the fitted values of $F_2^{\mathbb{R}}(\beta,Q^2)$ increase with decreasing $\beta$ such that they are consistent in shape with parameterisations of the pion structure function. Since the errors on the current data are insensitive to any $Q^2$ evolution of $F_2^{\mathbb{R}}(\beta,Q^2)$, the structure function of the subleading exchange is taken from a parameterisation of the pion [53] multiplied by a single coefficient $C_{\mathbb{R}}$ to be determined from the data.

No momentum sum rules are imposed because of the theoretical uncertainty in specifying the normalisation of the pomeron or meson fluxes ($f_{\mathbb{P}/p}(x_{\mathbb{P}}), f_{\mathbb{R}/p}(x_{\mathbb{P}})$) and because it is not clear that such a sum rule is appropriate for the parton distributions of a virtual exchange.

## 6.2   QCD Fits of $F_2^{D(3)}(x_{\mathbb{P}},\beta,Q^2)$

In the following fits the values of $F_2^{D(3)}(\beta,Q^2,x_{\mathbb{P}})$ are calculated from $F_2^{\mathbb{P}}(\beta,Q^2)$ and $F_2^{\mathbb{R}}(\beta,Q^2)$ using equation (14) assuming no interference between the leading and subleading trajectories. All QCD fits are performed using the combined statistical errors from the data and the Monte Carlo simulations. As in the phenomenological fits, the

data for $y > 0.45$ are excluded from all of the QCD fits to limit the uncertainty introduced by the lack of knowledge of $R^{D(5)}$. Data points corresponding to values of $M_X$ less than $2\,\mathrm{GeV}$ are also excluded because of the large contribution to the cross section from the resonant production of vector mesons and other possible higher twist contributions in this region.

For fit 1 only quarks are assumed to contribute to the structure of the pomeron at the starting scale of $Q_0^2 = 3\,\mathrm{GeV}^2$, and the values of $\alpha_{\mathbb{P}}(0)$ and $\alpha_{\mathbb{R}}(0)$ are fixed to those determined in the Regge fit without interference (fit B). The parameters to be fitted are then $C_j^q$ and the normalisation of the subleading component $C_{\mathbb{R}}$. Introducing successive terms from the Chebyshev series, a $\chi^2/\mathrm{ndf}$ of $314.2/159$ is reached for 3 terms. If an additional term is introduced then the corresponding coefficient is consistent with 0, with no improvement of the quality of the fit. The resulting parameterisation of $F_2^{D(3)}$ is shown at a constant value of $x_{\mathbb{P}} = 0.003$ as a function of $Q^2$ for different values of $\beta$ in figure 6(a), and as a function of $\beta$ at fixed $Q^2$ in figure 7(a). Also shown are the data for $x_{\mathbb{P}} F_2^{D(3)}$ interpolated to $x_{\mathbb{P}} = 0.003$ using fit B. The large $\chi^2/\mathrm{ndf}$ for fit 1 arises from the failure to reproduce the scaling violations of $F_2^{D(3)}(x_{\mathbb{P}}, \beta, Q^2)$, which rises with increasing $Q^2$ for $\beta < 0.9$. Therefore, the data cannot be described by a parameterisation in which the pomeron contains only quarks at $Q^2 = 3\,\mathrm{GeV}^2$.

In fit 2 the first term in the expansion of the gluon distribution is introduced as an additional fit parameter, and a significantly better description of the data is obtained ($\chi^2/\mathrm{ndf} = 186.7/156$). The description of the data improves further with the introduction of the next two terms in the series to give $\chi^2/\mathrm{ndf} = 176.3/154$ for $n = 3$ (fit 3). This fit is shown in figures 6(b) and 7(b) where it can be seen that the dependence of $F_2^{D(3)}(x_{\mathbb{P}}, \beta, Q^2)$ on $Q^2$ and $\beta$ is well reproduced. Introducing additional terms for the gluon distribution does not result in any further improvement of the quality of the fit.

The parton distributions resulting from fits 2 and 3 are shown in figure 8 where both the sum of the light quark distributions and the gluon distribution are shown for each fit at the lowest and highest $Q^2$ values included in the analysis as well as an intermediate value of $Q^2 = 12\,\mathrm{GeV}^2$. In both fits 2 and 3 the fraction of the momentum of the pomeron carried by gluons decreases with increasing $Q^2$ from $\sim 90\%$ at $Q^2 = 4.5\,\mathrm{GeV}^2$ to $\sim 80\%$ at $Q^2 = 75\,\mathrm{GeV}^2$. A large gluon component in the pomeron is, therefore, favoured by the data.

Repeating fit 3 with $\alpha_{\mathbb{P}}(0)$ and $\alpha_{\mathbb{R}}(0)$ as free parameters results in no change in either the coefficients $C_j^{q,g}$ or the quality of the fit, and the values for $\alpha_{\mathbb{P}}(0)$ and $\alpha_{\mathbb{R}}(0)$ are unchanged from those obtained in the Regge fit B. The parameters $a$ and $Q_0^2$ may be varied in fit 3 within the ranges $0 < a < 0.1$ and $2 < Q_0^2 < 4\,\mathrm{GeV}^2$ without producing a change of more than one unit in the $\chi^2$, and if $a$ is allowed to vary in the fit then the value obtained is consistent with 0.01. A final fit is performed to assess the influence of the particular choice of the meson structure function by reweighting the parameterisation of [53] by a factor $(1 - \beta)^{\gamma_{\mathbb{R}}}$. The value of $\gamma_{\mathbb{R}}$ obtained is consistent with zero.

## 6.3  Discussion of the QCD Fits

We conclude that it is possible to describe the data for $F_2^{D(3)}$ in the region $M_X > 2\,\text{GeV}$ with a factorisable model in which the pomeron structure function evolves with $Q^2$ according to the NLO DGLAP evolution equations. Within the context of this model a large gluonic content of the pomeron is required, with a hard distribution in fractional momentum in order to achieve an adequate description of the data. The data exhibit some preference for a gluon distribution that is large at high $z$ such that for low values of $Q^2$ the majority of the momentum of the pomeron is carried by a single gluon, although the precise shape of the gluon distribution is not well constrained. It should be noted, however, that there are some unresolved theoretical problems associated with the use of the DGLAP evolution equations at very large $z$ due to resummation effects [54], which may be particularly important when the parton densities near $z = 1$ are very large as in fit 3.

The fraction of the momentum of the pomeron carried by gluons is similar in both fits 2 and 3, from $\sim 90\%$ at $Q^2 = 4.5\,\text{GeV}^2$ to $\sim 80\%$ at $Q^2 = 75\,\text{GeV}^2$. Thus the data lend support to pictures of diffraction in DIS in which the dominant mechanism is boson-gluon fusion with the incoming gluon carrying a large fraction of the momentum of the pomeron [5,55].

Measurements of the properties of hadronic final states produced in diffractive hard interactions are essential to clarify the extent to which this partonic interpretation may be applied universally. For example, a large gluon distribution in the pomeron, peaked near $z = 1$, was found to describe well the measurements of diffractive dijet production in $p\bar{p}$ interactions [56]. The large gluon distribution favoured by the present analysis predicts a sizable cross section for diffractive dijet and charm production in both $pp$ and $ep$ interactions. To facilitate comparisons between such measurements [57] and the parton distribution functions presented here, parameterisations of the parton distributions functions for the NLO fits 1, 2 and 3 are available [44]. Parameterisations are also available of the results of three leading order QCD fits which are identical to the NLO fits 1, 2 and 3 in all other respects. The results of these additional fits, not shown here, lead to the same conclusions as those outlined above.

The QCD analysis of $F_2^{D(3)}$ presented in this paper does not attempt to address the physical origin within QCD of either the intercepts of the leading and subleading exchanges, or of the parton distributions at the starting scale of the perturbative evolution. It is hoped that a more complete understanding of colour singlet exchange interactions within QCD will establish the extent to which the DGLAP evolution prescription is appropriate, and also provide predictions for $\alpha_{\mathbb{P}}(0)$ and $\alpha_{\mathbb{R}}(0)$.

## 7  Summary

The differential structure function $F_2^{D(3)}(x_{\mathbb{P}}, \beta, Q^2)$ has been measured using the data taken in 1994 with the H1 detector with greater accuracy and over a greater kinematic range than previously. At this level of precision it is found that $F_2^{D(3)}$ is inconsistent with a universal dependence on $x_{\mathbb{P}}$. A natural explanation of this breaking of factorisation is presented in which a leading pomeron exchange is accompanied by a subleading meson

19

exchange. Fits to the data in which such a subleading term is considered yield an intercept for the pomeron of $\alpha_{\mathbb{P}}(0) = 1.203 \pm 0.020(\text{stat.}) \pm 0.013(\text{sys.})^{+0.030}_{-0.035}(\text{model})$, which is significantly higher than the value obtained in similar parameterisations of soft hadronic cross sections. No evidence is found for any variation of $\alpha_{\mathbb{P}}(0)$ with $Q^2$ or $\beta$ in the range $4.5 < Q^2 < 75\,\text{GeV}^2$ and $0.04 < \beta < 0.9$. The value obtained for the intercept for the subleading exchange, $\alpha_{\mathbb{R}}(0) = 0.50 \pm 0.11(\text{stat.}) \pm 0.11(\text{sys.})^{+0.09}_{-0.10}(\text{model})$, was found to agree well with values obtained from soft hadronic scattering processes.

A model in which the deep-inelastic structure of the leading exchange is described by parton distributions which evolve according to the NLO DGLAP evolution equations is consistent with the data for $F_2^{D(3)}(x_{\mathbb{P}}, \beta, Q^2)$ in the region $M_X > 2\,\text{GeV}$. Under such a hypothesis, the data require approximately 90% and 80% of the momentum of the pomeron to be carried by gluons at $Q^2 = 4.5\,\text{GeV}^2$ and $Q^2 = 75\,\text{GeV}^2$ respectively. A parametrisation which assumes only quarks in the diffractive exchange at $Q^2 = 3\,\text{GeV}^2$ is excluded.

# Acknowledgements

# References

[1] T. Regge, Nuov. Cim. 14 (1959) 951, Nuov. Cim. 18 (1960) 947.

[2] G. Chew, S. Frautschi, S. Mandelstam, Phys. Rev. 126 (1962) 1202.

[3] G. Chew, S. Frautschi, Phys. Rev. Lett. 7 (1961) 394.

[4] L. N. Lipatov, DESY 96-132 (1996).

[5] A. R. White, ANL-HEP-CP-96-74 (1996).

[6] ZEUS Collaboration, M.Derrick et al., Phys. Lett. B315 (1993) 481.

[7] H1 Collaboration, T. Ahmed et al., Nucl. Phys. B429 (1994) 477.

[8] H1 Collaboration, T. Ahmed et al., Phys. Lett. B348 (1995) 681.

[9] ZEUS Collaboration, M.Derrick et al., Z. Phys. C68 (1995) 569.

[10] A. Donnachie, P.V. Landshoff, Phys. Lett. B191 (1987) 309.

[11] G. Ingelman, K. Janson-Prytz, Proceedings of the Workshop on "Physics at HERA", vol. 1, eds. W. Buchmüller, G. Ingelman, DESY (1992) p.233.
G. Ingelman, K. Prytz, Z. Phys. C58 (1993) 285.

[12] H. Jung, Comp. Phys. Comm. 86 (1995) 147.

[13] P. Collins, "An Introduction to Regge Theory & High Energy Physics ", Cambridge University Press, Cambridge (1977).

[14] E. Barberis, Proceedings of Workshop on "Deep-Inelastic Scattering and QCD", eds. G. D'Agostini and A. Nigro, Rome, (1996) p 343.

[15] A. Kaidalov, Phys. Rep. 50 (1979) 157.

[16] W. Apel et al., Nucl. Phys. B154 (1979) 189.

[17] M. Glück, E. Reya, A. Vogt, Z. Phys. C53 (1992) 651.

[18] Yu. L. Dokshitzer, JETP 46 (1977) 641.
V. N. Gribov, L. N. Lipatov, Sov. Journ. Nucl. Phys. 15 (1972) 78.
G. Altarelli, G. Parisi, Nucl. Phys. B126 (1977) 298.

[19] L. Lönnblad, Computer Phys. Comm. 71 (1992) 15.

[20] G. Ingelman, Proceedings of the Workshop on "Physics at HERA", vol. 3, eds. W. Buchmüller, G. Ingelman, DESY (1992) p.1366.

[21] A. Kwiatkowski, H. Spiesberger, H.-J. Möhring, Computer Phys. Comm. 69 (1992) 155.

[22] B. List, "Diffraktive $J/\psi$−Produktion in Elektron-Proton-Stößen am Speicherring HERA", Diploma Thesis (Tech. Univ. Berlin), 1993 (unpublished).

[23] H1 Collaboration, S. Aid et al., Nucl. Phys. B468 (1996) 3.

[24] NMC Collaboration, M. Arneodo et al., Nucl. Phys. B429 (1994) 503.

[25] ZEUS Collaboration, M. Derrick et al., Phys. Lett. B380 (1996) 220.

[26] H1 Collaboration, C. Adloff et al., DESY 97-082 (May 1997).

[27] K. Goulianos, Phys. Rep. 101 (1983) 169.

[28] T. Sjöstrand, CERN−TH.7112/93 (1993) (revised February 1994).

[29] Z. Koba, H. Nielsen, P. Olesen, Nucl. Phys. B40 (1972) 317.

[30] G. A. Schuler, H. Spiesberger, Proceedings of the Workshop on "Physics at HERA", vol. 3, eds. W. Buchmüller, G. Ingelman, DESY (1992) p.1419.

[31] H1 Collaboration, I. Abt et al., Z. Phys. C63 (1994) 377.

[32] H1 Collaboration, T. Ahmed et al., Nucl. Phys. B470 (1996) 3.

[33] R. Engel, Z. Phys. C66 (1995) 203.
R. Engel, J. Ranft, Phys. Rev. D54 (1996) 4244.

[34] H1 Collaboration, S. Aid et al., Z. Phys. C69 (1995) 27.

[35] A. Courau, P. Kessler, Phys. Rev. D46 (1992) 117.

[36] H1 Collaboration, I. Abt et al., Nucl. Instr. and Meth. A386 (1997) 310 and 348.

[37] A. Mehta, "Measurement of the Diffractive Proton Structure Function and Calibration of the Forward Muon Detector at H1", PhD thesis (Univ. Manchester), 1994 (Unpublished).

[38] H1 Collaboration, C. Adloff et al., Z. Phys. C74 (1997) 221.

[39] K. C. Hoeger, in Proceedings of the Workshop "Physics at HERA", vol. 1, p. 43, ed. W. Buchmüller and G. Ingelman, DESY (1992) p.43.

[40] F. Jacquet, A. Blondel, in Proceedings of the Workshop "An ep facility for Europe", ed. U. Amaldi, (1979) p.391.

[41] U. Bassler, G. Bernardi, Nucl. Instr. and Meth. A361 (1995) 197.

[42] V. Hudgson, "Measurement of the Cross Section for the Quasi-elastic Photoproduction of $\psi(2S)$ at HERA", Ph.D. thesis (Univ. Birmingham), 1997 (Unpublished).

[43] H1 Collaboration, S. Aid et al., Phys. Lett. B338 (1994) 507.

[44] The table of results and parameterisations of both the leading and next-to-leading order fits discussed in this publication are available from $http : //dice2.desy.de/h1/www/h1work/dif/h1f2d1994.html$.

[45] A. Donnachie, P. Landshoff, Nucl. Phys. B303 (1988) 634.

[46] CDF Collaboration, F. Abe et al., Phys. Rev. D50 (1994) 5518.

[47] A. Donnachie, P. Landshoff, Phys. Lett. B296 (1992) 227.

[48] J. Cudell, K. Kang, S. Kim, Phys. Lett. B395 (1997) 311.

[49] G. Ingelman, P. Schlein, Phys. Lett. B152 (1985) 256.

[50] L. Trentadue, G. Veneziano, Phys. Lett. B323 (1994) 201.

[51] M.F. McDermott, G. Briskin, Proceedings of the Workshop on "Future Physics at HERA", ed. G. Ingelman, A. De Roeck, R. Klanner DESY (1996) p.691.

[52] M. Glück, E. Hoffmann, E. Reya, Z. Phys. C13 (1982) 119.
M. Glück, E. Reya, M. Stratmann, Nucl. Phys. B422 (1994) 37.

[53] J. F. Owens, Phys. Rev. D30 (1984) 943.

[54] D. Amati et. al., Nucl. Phys. B173 (1980) 429.
M. Ciafaloni, G. Curci, Phys. Lett. B102 (1981) 352.

[55] W. Buchmüller, A. Hebecker, Phys. Lett. B355 (1995) 573.

[56] UA8 Collaboration, A. Brandt et al., Phys. Lett. B297 (1992) 417.

[57] CDF Collaboration, F. Abe et al., Phys. Rev. Lett. 78 (1997) 2698.
CDF Collaboration, F. Abe et al., FERMILAB-PUB-97/076-E (1997).
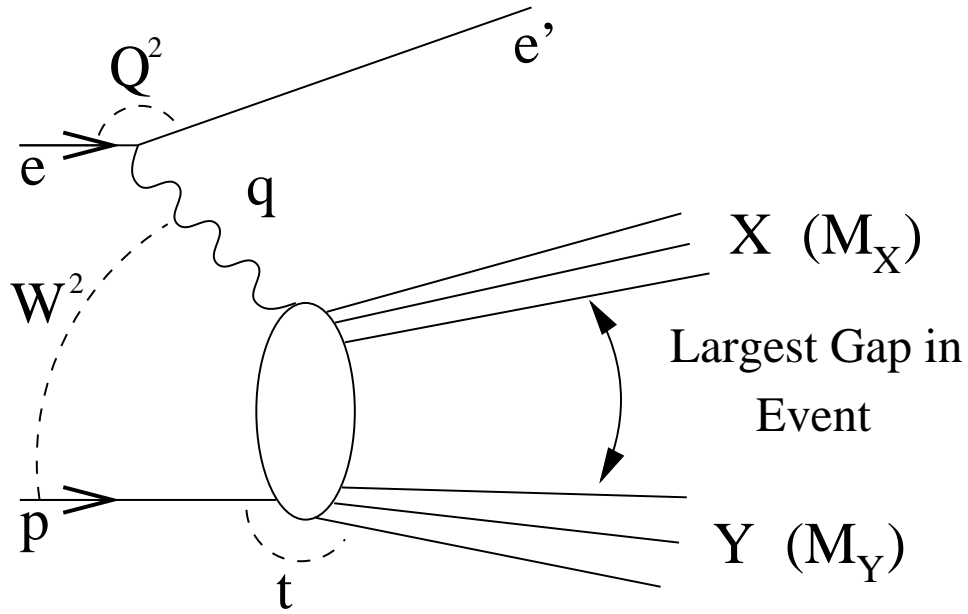
**Figure** 1: Schematic of an DIS scattering event $ep \rightarrow eXY$.
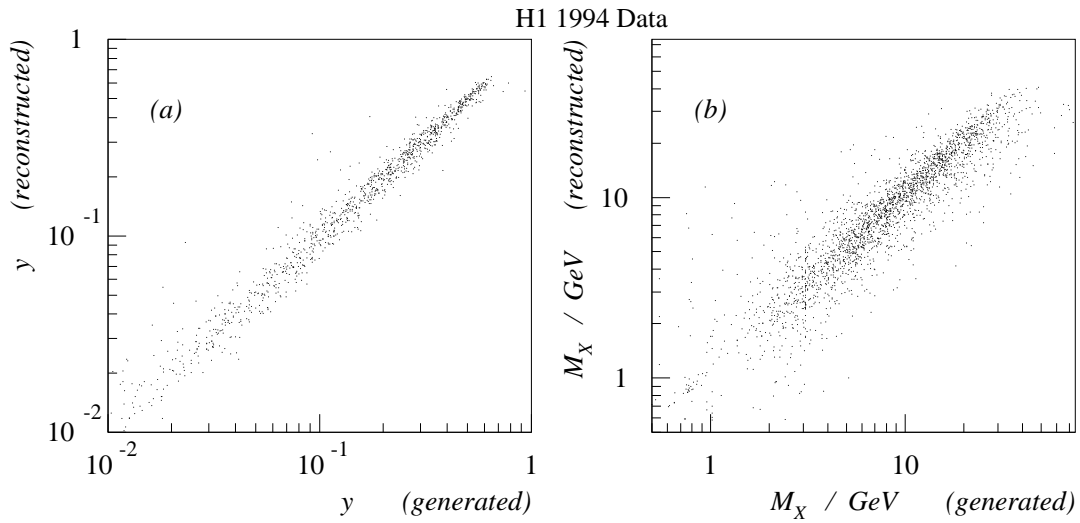


**Figure** 2: The correlation between the generated and reconstructed values of (a) $y$ (reconstructed using the weighted average method) and (b) $M_X$ for simulated Monte Carlo mixture at nominal vertex.
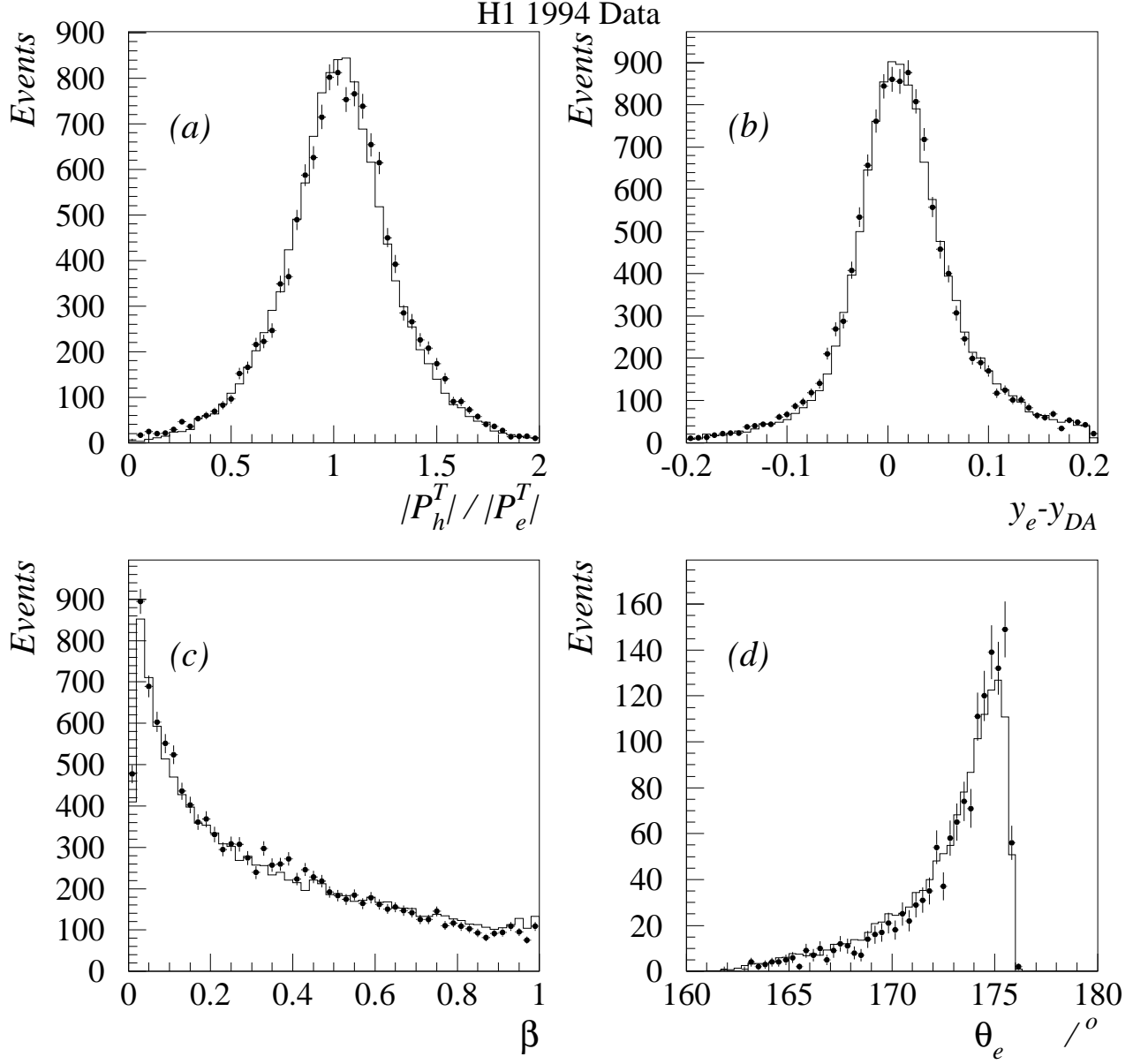
**Figure** 3: The solid points show (a) the ratio of the transverse momentum of the hadrons to that of the electron, (b) the difference between $y$ calculated from the electron and double angle methods, (c) the $\beta$ distribution and (d) the electron polar angle distribution. All distributions are shown for the rapidity gap DIS event sample. Plots (a), (b) and (c) are for the nominal vertex data and plot (d) is for the shifted vertex data. None of the distributions have been corrected for detector effects. The predictions from the simulation are shown for each plot as a solid histogram.

# H1 1994 Data
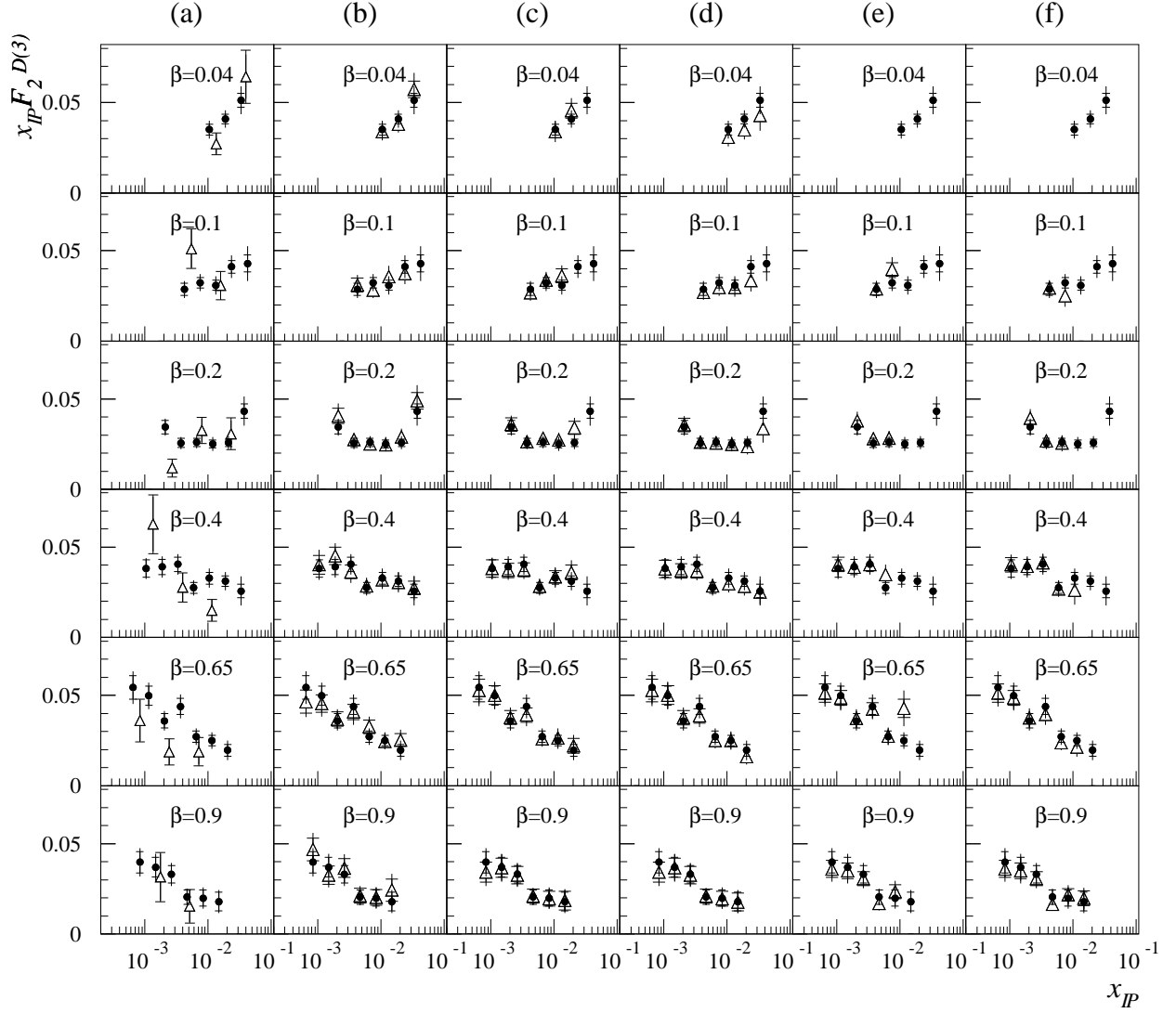


**Figure** 4: Effect of changing kinematic reconstruction techniques and rapidity gap selection criteria on the measured values of $x_{I\!P} F_2^{D(3)}$ at an example $Q^2$ value of $18\,\mathrm{GeV}^2$. The solid circles show the data measured using the standard analysis. In each of the six columns, these data are compared to those obtained with a modified analysis technique in which, (a) the shifted vertex data are compared (b) $x$ and $Q^2$ were reconstructed with the $\Sigma$ method and $M_x$ solely from the hadronic final state, (c) cut 10 (see table 1) is changed to $\eta_{\max}^{\mathrm{LAr}} < 3$, (d) cut 10 is not used, (e) cut 10 is replaced by $\eta_{\max}^{\mathrm{LAr}} < 2$ and there is no requirement on the forward detectors (i.e. cuts 11–13 are not applied), (f) there is no rapidity gap selection at all (i.e. cuts 10–13 are not applied). The comparisons are plotted only for those bins satisfying the minimum acceptance and purity limits as for the standard analysis.
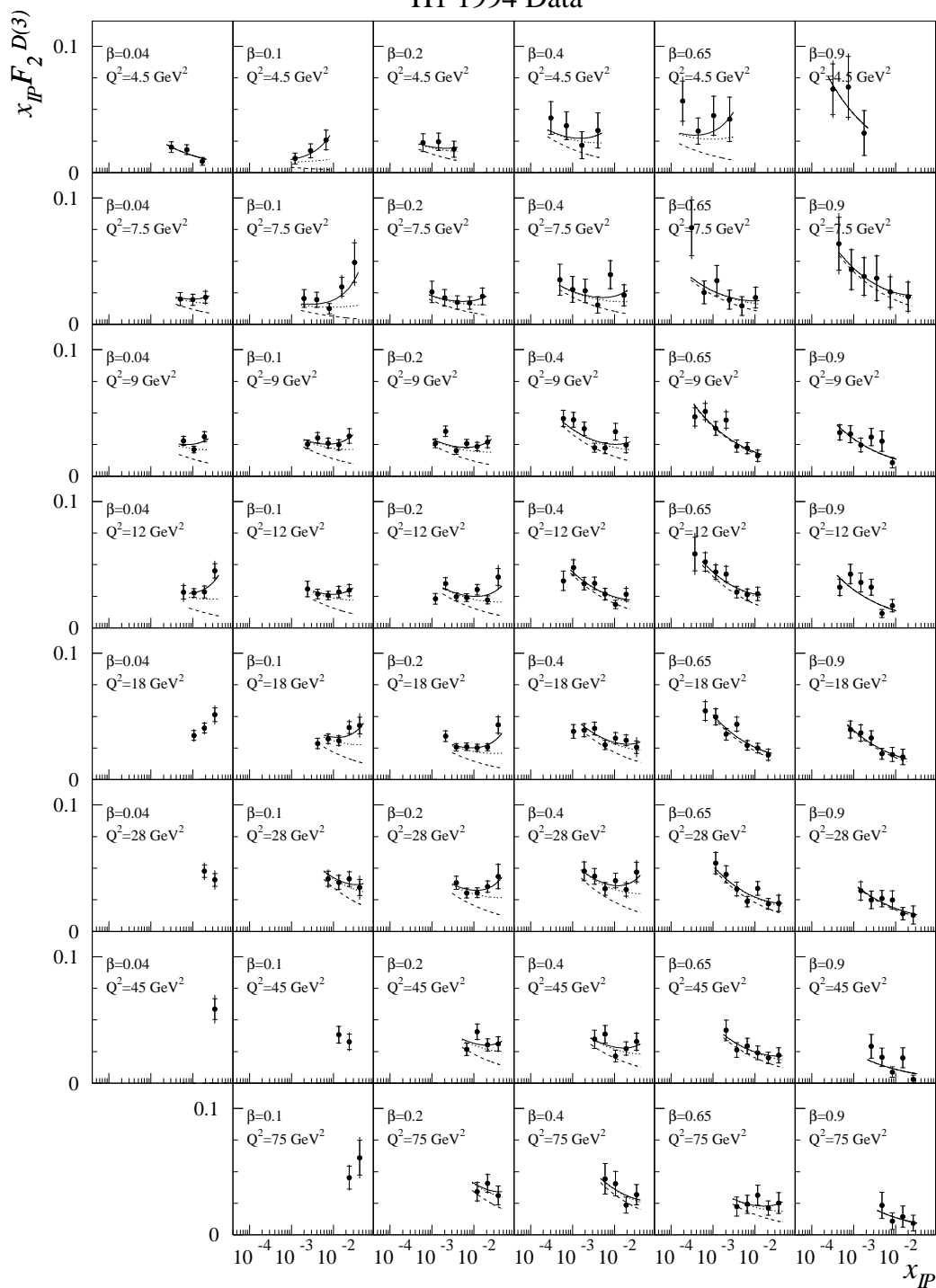
**Figure** 5: The solid points show the measured differential structure function plotted as $x_{I\!P} F_2^{D(3)}(x_{I\!P}, \beta, Q^2)$ against $x_{I\!P}$ for various $\beta$ and $Q^2$ values. The inner error bars represent the statistical errors and the outer error bars represent the statistical and systematic errors added in quadrature. The curves show the results of the Regge fit with interference (fit C) described in the text. The dashed curve is the contribution from the pomeron alone, the dotted curve is the pomeron plus interference and the continuous curve is the total contribution. The data that lie at values of $x_{I\!P}$ smaller than the extent of the curves have $y > 0.45$ and are excluded from the fit.

# H1 1994
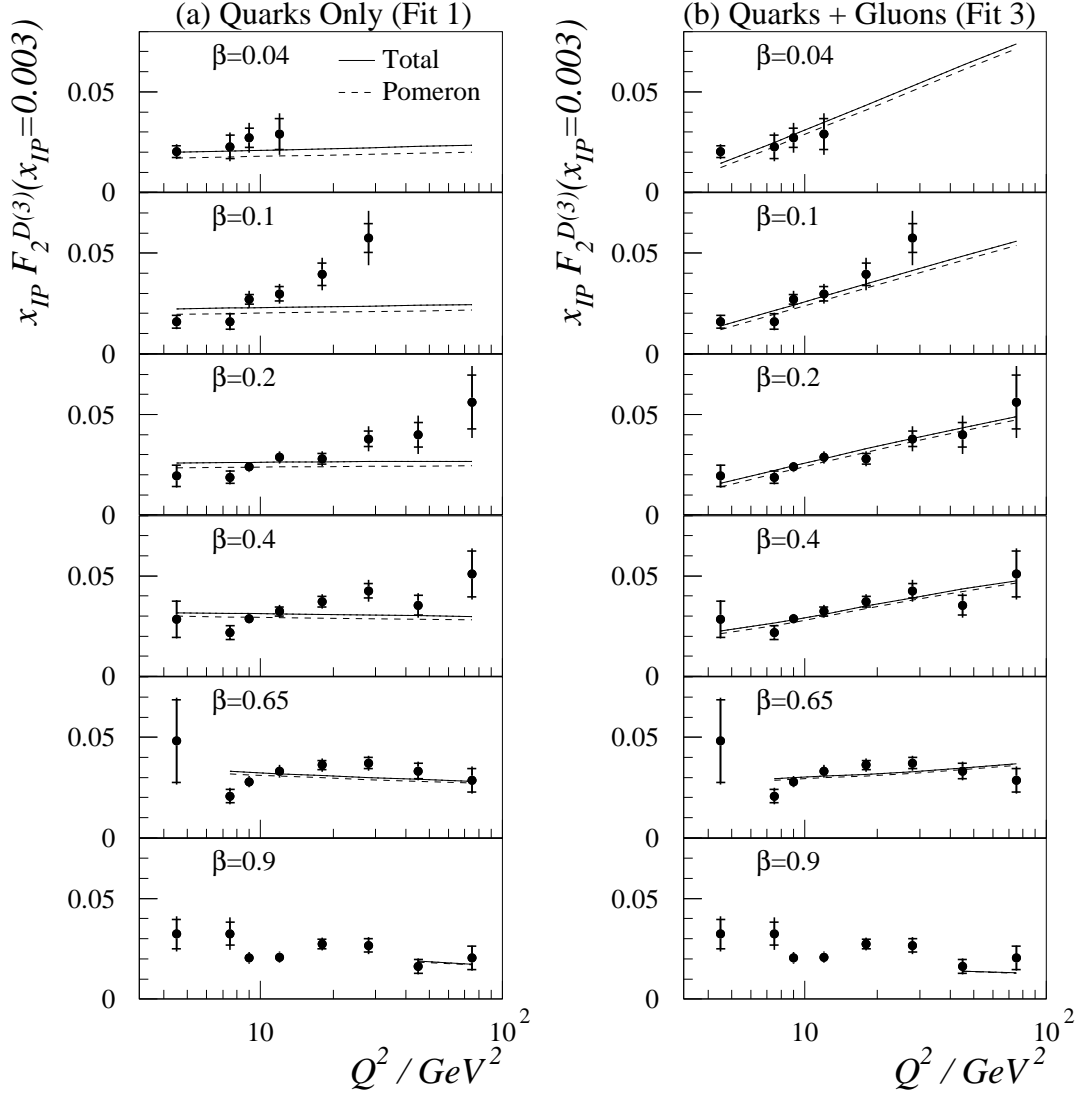


**Figure** 6: The quantity $x_{\mathbb{P}} F_2^{D(3)}(x_{\mathbb{P}}, \beta, Q^2)$ at $x_{\mathbb{P}} = 0.003$ as a function of $Q^2$ for different values of $\beta$. In both (a) and (b) the solid points show the same data, interpolated to $x_{\mathbb{P}} = 0.003$ using fit B (see text). In (a) the result of QCD fit 1 (in which only quarks contribute to the pomeron structure at $Q^2 = 3\,\text{GeV}^2$) is superimposed. In (b) the preferred QCD fit 3 (in which both quarks and gluons contribute) is shown. The results of the QCD fits are only shown in the kinematic range used in the fit (corresponding to data for which $M_X > 2\,\text{GeV}$). In both figures the solid line represents the value of $F_2^{D(3)}(x_{\mathbb{P}}, \beta, Q^2)$, whilst the dotted line shows the contribution from the pomeron term only.

27

# H1 1994



**Figure** 7: The quantity $x_{I\!P} F_2^{D(3)}(x_{I\!P}, \beta, Q^2)$ at $x_{I\!P} = 0.003$ as a function of $\beta$ for different values of $Q^2$. In both (a) and (b) the solid points show the same data, interpolated to $x_{I\!P} = 0.003$ using fit B (see text). In (a) the result of QCD fit 1 (in which only quarks contribute to the pomeron structure at $Q^2 = 3\,\text{GeV}^2$) is superimposed. In (b) the preferred QCD fit 3 (in which both quarks and gluons contribute) is shown. The results of the QCD fits are only shown in the kinematic range used in the fit (corresponding to data for which $M_x > 2\,\text{GeV}$). In both figures the solid line represents the value of $F_2^{D(3)}(x_{I\!P}, \beta, Q^2)$, whilst the dotted line shows the contribution from the pomeron term only.

28
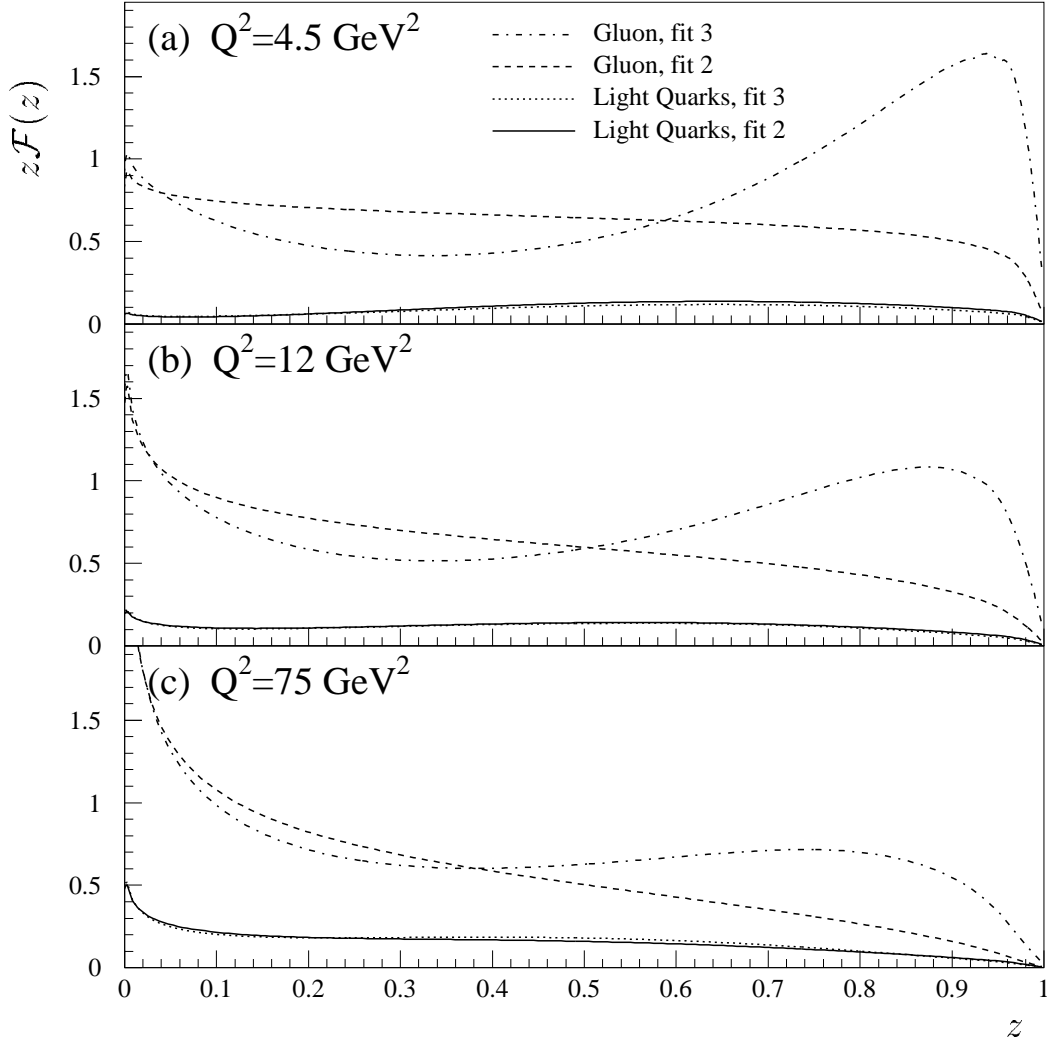
**Figure** 8: The sum of the light quark distributions and the gluon distribution for fits 2 and 3, shown at (a) $Q^2 = 4.5\,\mathrm{GeV}^2$, (b) $Q^2 = 12\,\mathrm{GeV}^2$ and (c) $Q^2 = 75\,\mathrm{GeV}^2$. In fit 2 the gluon distribution is parameterised at the starting scale $Q_0^2 = 3\,\mathrm{GeV}^2$ with only the first term in the polynomial expansion, while in fit 3 the first 3 terms are included. In both fits 3 polynomials are used to parameterise the light quark distribution. The figures are normalised such that they represent the parton distributions multiplied by the flux factor at $x_{\mathrm{I\!P}} = 0.003$.

| $Q^2$ | $\beta$ | $x$ | $x_{\mathbb{P}} F_2^{D(3)}$ | $\delta_{stat}$ | $\delta_{sys}$ |
|---|---|---|---|---|---|
| 4.5 | 0.04 | 0.00012 | 0.0203 | 0.0042 | 0.0017 |
| 4.5 | 0.04 | 0.00029 | 0.0182 | 0.0039 | 0.0017 |
| 4.5 | 0.04 | 0.00067 | 0.0091 | 0.0030 | 0.0017 |
| 4.5 | 0.10 | 0.00012 | 0.0112 | 0.0044 | 0.0015 |
| 4.5 | 0.10 | 0.00029 | 0.0174 | 0.0055 | 0.0025 |
| 4.5 | 0.10 | 0.00067 | 0.0259 | 0.0077 | 0.0038 |
| 4.5 | 0.20 | 0.00012 | 0.0238 | 0.0070 | 0.0022 |
| 4.5 | 0.20 | 0.00029 | 0.0246 | 0.0068 | 0.0021 |
| 4.5 | 0.20 | 0.00067 | 0.0185 | 0.0063 | 0.0024 |
| 4.5 | 0.40 | 0.00012 | 0.0433 | 0.0130 | 0.0033 |
| 4.5 | 0.40 | 0.00029 | 0.0372 | 0.0110 | 0.0015 |
| 4.5 | 0.40 | 0.00067 | 0.0218 | 0.0107 | 0.0022 |
| 4.5 | 0.40 | 0.00160 | 0.0335 | 0.0139 | 0.0039 |
| 4.5 | 0.65* | 0.00012 | 0.0566 | 0.0159 | 0.0112 |
| 4.5 | 0.65* | 0.00029 | 0.0330 | 0.0104 | 0.0032 |
| 4.5 | 0.65* | 0.00067 | 0.0451 | 0.0154 | 0.0055 |
| 4.5 | 0.65* | 0.00160 | 0.0423 | 0.0175 | 0.0049 |
| 4.5 | 0.90* | 0.00029 | 0.0660 | 0.0200 | 0.0105 |
| 4.5 | 0.90* | 0.00067 | 0.0678 | 0.0242 | 0.0109 |
| 4.5 | 0.90* | 0.00160 | 0.0314 | 0.0177 | 0.0044 |
| 7.5 | 0.04 | 0.00020 | 0.0201 | 0.0053 | 0.0011 |
| 7.5 | 0.04 | 0.00040 | 0.0195 | 0.0043 | 0.0027 |
| 7.5 | 0.04 | 0.00079 | 0.0215 | 0.0046 | 0.0039 |
| 7.5 | 0.10 | 0.00020 | 0.0205 | 0.0071 | 0.0021 |
| 7.5 | 0.10 | 0.00040 | 0.0195 | 0.0060 | 0.0019 |
| 7.5 | 0.10 | 0.00079 | 0.0124 | 0.0042 | 0.0013 |
| 7.5 | 0.10 | 0.00158 | 0.0298 | 0.0074 | 0.0056 |
| 7.5 | 0.10 | 0.00316 | 0.0490 | 0.0156 | 0.0101 |
| 7.5 | 0.20 | 0.00020 | 0.0258 | 0.0085 | 0.0019 |
| 7.5 | 0.20 | 0.00040 | 0.0210 | 0.0065 | 0.0023 |
| 7.5 | 0.20 | 0.00079 | 0.0174 | 0.0054 | 0.0016 |
| 7.5 | 0.20 | 0.00158 | 0.0170 | 0.0050 | 0.0021 |
| 7.5 | 0.20 | 0.00316 | 0.0222 | 0.0065 | 0.0034 |
| 7.5 | 0.40 | 0.00020 | 0.0354 | 0.0123 | 0.0028 |
| 7.5 | 0.40 | 0.00040 | 0.0277 | 0.0102 | 0.0014 |
| 7.5 | 0.40 | 0.00079 | 0.0266 | 0.0092 | 0.0026 |
| 7.5 | 0.40 | 0.00158 | 0.0155 | 0.0064 | 0.0010 |
| 7.5 | 0.40 | 0.00316 | 0.0394 | 0.0110 | 0.0048 |
| 7.5 | 0.40 | 0.00668 | 0.0231 | 0.0083 | 0.0036 |
| 7.5 | 0.65 | 0.00020 | 0.0764 | 0.0221 | 0.0116 |
| 7.5 | 0.65 | 0.00040 | 0.0253 | 0.0091 | 0.0026 |
| 7.5 | 0.65 | 0.00079 | 0.0347 | 0.0120 | 0.0029 |
| 7.5 | 0.65 | 0.00158 | 0.0196 | 0.0076 | 0.0024 |
| 7.5 | 0.65 | 0.00316 | 0.0146 | 0.0074 | 0.0025 |
| 7.5 | 0.65 | 0.00668 | 0.0212 | 0.0082 | 0.0034 |
| 7.5 | 0.90* | 0.00040 | 0.0638 | 0.0209 | 0.0122 |
| 7.5 | 0.90* | 0.00079 | 0.0434 | 0.0158 | 0.0063 |
| 7.5 | 0.90* | 0.00158 | 0.0379 | 0.0148 | 0.0071 |
| 7.5 | 0.90* | 0.00316 | 0.0365 | 0.0177 | 0.0062 |
| 7.5 | 0.90* | 0.00668 | 0.0257 | 0.0121 | 0.0077 |
| 7.5 | 0.90* | 0.01778 | 0.0220 | 0.0116 | 0.0064 |
| 9.0 | 0.04 | 0.00024 | 0.0279 | 0.0035 | 0.0027 |
| 9.0 | 0.04 | 0.00042 | 0.0211 | 0.0026 | 0.0020 |
| 9.0 | 0.04 | 0.00075 | 0.0313 | 0.0040 | 0.0027 |
| 9.0 | 0.10 | 0.00024 | 0.0252 | 0.0035 | 0.0019 |
| 9.0 | 0.10 | 0.00042 | 0.0304 | 0.0042 | 0.0033 |

| $Q^2$ | $\beta$ | $x$ | $x_{\mathbb{P}} F_2^{D(3)}$ | $\delta_{stat}$ | $\delta_{sys}$ |
|---|---|---|---|---|---|
| 9.0 | 0.10 | 0.00075 | 0.0261 | 0.0039 | 0.0030 |
| 9.0 | 0.10 | 0.00133 | 0.0248 | 0.0041 | 0.0029 |
| 9.0 | 0.10 | 0.00237 | 0.0317 | 0.0057 | 0.0034 |
| 9.0 | 0.20 | 0.00024 | 0.0260 | 0.0035 | 0.0016 |
| 9.0 | 0.20 | 0.00042 | 0.0354 | 0.0041 | 0.0022 |
| 9.0 | 0.20 | 0.00075 | 0.0200 | 0.0026 | 0.0018 |
| 9.0 | 0.20 | 0.00133 | 0.0257 | 0.0034 | 0.0015 |
| 9.0 | 0.20 | 0.00237 | 0.0235 | 0.0033 | 0.0028 |
| 9.0 | 0.20 | 0.00421 | 0.0270 | 0.0046 | 0.0030 |
| 9.0 | 0.40 | 0.00024 | 0.0456 | 0.0064 | 0.0029 |
| 9.0 | 0.40 | 0.00042 | 0.0446 | 0.0060 | 0.0028 |
| 9.0 | 0.40 | 0.00075 | 0.0375 | 0.0053 | 0.0029 |
| 9.0 | 0.40 | 0.00133 | 0.0226 | 0.0035 | 0.0013 |
| 9.0 | 0.40 | 0.00237 | 0.0222 | 0.0044 | 0.0014 |
| 9.0 | 0.40 | 0.00421 | 0.0351 | 0.0066 | 0.0025 |
| 9.0 | 0.40 | 0.00750 | 0.0247 | 0.0061 | 0.0032 |
| 9.0 | 0.65 | 0.00024 | 0.0469 | 0.0072 | 0.0059 |
| 9.0 | 0.65 | 0.00042 | 0.0511 | 0.0065 | 0.0057 |
| 9.0 | 0.65 | 0.00075 | 0.0378 | 0.0054 | 0.0028 |
| 9.0 | 0.65 | 0.00133 | 0.0445 | 0.0065 | 0.0051 |
| 9.0 | 0.65 | 0.00237 | 0.0238 | 0.0047 | 0.0024 |
| 9.0 | 0.65 | 0.00421 | 0.0222 | 0.0044 | 0.0029 |
| 9.0 | 0.65 | 0.00750 | 0.0161 | 0.0044 | 0.0030 |
| 9.0 | 0.90* | 0.00042 | 0.0346 | 0.0061 | 0.0034 |
| 9.0 | 0.90* | 0.00075 | 0.0332 | 0.0066 | 0.0032 |
| 9.0 | 0.90* | 0.00133 | 0.0246 | 0.0055 | 0.0030 |
| 9.0 | 0.90* | 0.00237 | 0.0310 | 0.0068 | 0.0024 |
| 9.0 | 0.90* | 0.00421 | 0.0277 | 0.0080 | 0.0031 |
| 9.0 | 0.90* | 0.00750 | 0.0106 | 0.0041 | 0.0012 |
| 12.0 | 0.04 | 0.00024 | 0.0281 | 0.0054 | 0.0050 |
| 12.0 | 0.04 | 0.00042 | 0.0277 | 0.0034 | 0.0023 |
| 12.0 | 0.04 | 0.00075 | 0.0284 | 0.0047 | 0.0028 |
| 12.0 | 0.04 | 0.00133 | 0.0452 | 0.0056 | 0.0056 |
| 12.0 | 0.10 | 0.00024 | 0.0308 | 0.0061 | 0.0028 |
| 12.0 | 0.10 | 0.00042 | 0.0268 | 0.0038 | 0.0022 |
| 12.0 | 0.10 | 0.00075 | 0.0256 | 0.0033 | 0.0017 |
| 12.0 | 0.10 | 0.00133 | 0.0285 | 0.0045 | 0.0030 |
| 12.0 | 0.10 | 0.00237 | 0.0298 | 0.0044 | 0.0033 |
| 12.0 | 0.20 | 0.00024 | 0.0230 | 0.0042 | 0.0015 |
| 12.0 | 0.20 | 0.00042 | 0.0351 | 0.0045 | 0.0030 |
| 12.0 | 0.20 | 0.00075 | 0.0248 | 0.0031 | 0.0018 |
| 12.0 | 0.20 | 0.00133 | 0.0239 | 0.0031 | 0.0015 |
| 12.0 | 0.20 | 0.00237 | 0.0302 | 0.0041 | 0.0022 |
| 12.0 | 0.20 | 0.00421 | 0.0222 | 0.0033 | 0.0022 |
| 12.0 | 0.20 | 0.00750 | 0.0403 | 0.0068 | 0.0068 |
| 12.0 | 0.40 | 0.00024 | 0.0372 | 0.0077 | 0.0033 |
| 12.0 | 0.40 | 0.00042 | 0.0478 | 0.0060 | 0.0039 |
| 12.0 | 0.40 | 0.00075 | 0.0351 | 0.0050 | 0.0026 |
| 12.0 | 0.40 | 0.00133 | 0.0354 | 0.0049 | 0.0025 |
| 12.0 | 0.40 | 0.00237 | 0.0267 | 0.0046 | 0.0026 |
| 12.0 | 0.40 | 0.00421 | 0.0186 | 0.0034 | 0.0018 |
| 12.0 | 0.40 | 0.00750 | 0.0266 | 0.0047 | 0.0047 |
| 12.0 | 0.65 | 0.00024 | 0.0585 | 0.0133 | 0.0100 |
| 12.0 | 0.65 | 0.00042 | 0.0523 | 0.0072 | 0.0044 |
| 12.0 | 0.65 | 0.00075 | 0.0442 | 0.0057 | 0.0045 |
| 12.0 | 0.65 | 0.00133 | 0.0425 | 0.0061 | 0.0043 |

**Table 3:** The quantity $x_{\mathbb{P}} F_2^{D(3)}$ as a function of $x$, $\beta$ and $Q^2$ together with the statistical and systematic errors. Not included in the errors are separate overall normalisation uncertainties of $\pm 6.0\%$ for the data with $Q^2 < 9\,\mathrm{GeV}^2$ and $\pm 4.8\%$ for those with $Q^2 \geq 9\,\mathrm{GeV}^2$. The data marked with an asterix correspond to the cross section, $\frac{\mathrm{d}^3 \sigma_{ep \to eXY}}{\mathrm{d}x\,\mathrm{d}\beta\,\mathrm{d}Q^2}$, averaged across the bin in $\beta$. The $\beta$ boundaries for these data are 0.5 and 0.8 for the bins at $\beta = 0.65$, and 0.8 and 1.0 for the bins at $\beta = 0.9$.

| $Q^2$ | $\beta$ | $x$ | $x_{\mathbb{P}} F_2^{D(3)}$ | $\delta_{stat}$ | $\delta_{sys}$ | $Q^2$ | $\beta$ | $x$ | $x_{\mathbb{P}} F_2^{D(3)}$ | $\delta_{stat}$ | $\delta_{sys}$ |
|---|---|---|---|---|---|---|---|---|---|---|---|
| 12.0 | 0.65 | 0.00237 | 0.0284 | 0.0045 | 0.0023 | 28.0 | 0.40 | 0.00421 | 0.0401 | 0.0057 | 0.0028 |
| 12.0 | 0.65 | 0.00421 | 0.0264 | 0.0044 | 0.0032 | 28.0 | 0.40 | 0.00750 | 0.0331 | 0.0053 | 0.0042 |
| 12.0 | 0.65 | 0.00750 | 0.0269 | 0.0054 | 0.0028 | 28.0 | 0.40 | 0.01330 | 0.0470 | 0.0078 | 0.0058 |
| 12.0 | 0.90* | 0.00042 | 0.0321 | 0.0064 | 0.0042 | 28.0 | 0.65 | 0.00075 | 0.0539 | 0.0084 | 0.0043 |
| 12.0 | 0.90* | 0.00075 | 0.0426 | 0.0076 | 0.0037 | 28.0 | 0.65 | 0.00133 | 0.0451 | 0.0066 | 0.0035 |
| 12.0 | 0.90* | 0.00133 | 0.0359 | 0.0075 | 0.0032 | 28.0 | 0.65 | 0.00237 | 0.0335 | 0.0053 | 0.0032 |
| 12.0 | 0.90* | 0.00237 | 0.0322 | 0.0064 | 0.0019 | 28.0 | 0.65 | 0.00421 | 0.0236 | 0.0041 | 0.0018 |
| 12.0 | 0.90* | 0.00421 | 0.0114 | 0.0033 | 0.0011 | 28.0 | 0.65 | 0.00750 | 0.0341 | 0.0054 | 0.0026 |
| 12.0 | 0.90* | 0.00750 | 0.0176 | 0.0050 | 0.0018 | 28.0 | 0.65 | 0.01330 | 0.0217 | 0.0042 | 0.0024 |
| 18.0 | 0.04 | 0.00042 | 0.0350 | 0.0039 | 0.0031 | 28.0 | 0.65 | 0.02370 | 0.0223 | 0.0063 | 0.0042 |
| 18.0 | 0.04 | 0.00075 | 0.0408 | 0.0039 | 0.0030 | 28.0 | 0.90* | 0.00133 | 0.0321 | 0.0072 | 0.0042 |
| 18.0 | 0.04 | 0.00133 | 0.0513 | 0.0054 | 0.0055 | 28.0 | 0.90* | 0.00237 | 0.0249 | 0.0069 | 0.0027 |
| 18.0 | 0.10 | 0.00042 | 0.0286 | 0.0041 | 0.0024 | 28.0 | 0.90* | 0.00421 | 0.0260 | 0.0065 | 0.0017 |
| 18.0 | 0.10 | 0.00075 | 0.0323 | 0.0038 | 0.0027 | 28.0 | 0.90* | 0.00750 | 0.0249 | 0.0072 | 0.0030 |
| 18.0 | 0.10 | 0.00133 | 0.0309 | 0.0038 | 0.0033 | 28.0 | 0.90* | 0.01330 | 0.0140 | 0.0050 | 0.0013 |
| 18.0 | 0.10 | 0.00237 | 0.0411 | 0.0047 | 0.0043 | 28.0 | 0.90* | 0.02370 | 0.0129 | 0.0071 | 0.0020 |
| 18.0 | 0.10 | 0.00421 | 0.0429 | 0.0066 | 0.0070 | 45.0 | 0.04 | 0.00133 | 0.0585 | 0.0081 | 0.0078 |
| 18.0 | 0.20 | 0.00042 | 0.0344 | 0.0042 | 0.0021 | 45.0 | 0.10 | 0.00133 | 0.0384 | 0.0066 | 0.0030 |
| 18.0 | 0.20 | 0.00075 | 0.0256 | 0.0030 | 0.0015 | 45.0 | 0.10 | 0.00237 | 0.0328 | 0.0061 | 0.0043 |
| 18.0 | 0.20 | 0.00133 | 0.0261 | 0.0030 | 0.0018 | 45.0 | 0.20 | 0.00133 | 0.0268 | 0.0049 | 0.0023 |
| 18.0 | 0.20 | 0.00237 | 0.0251 | 0.0028 | 0.0027 | 45.0 | 0.20 | 0.00237 | 0.0406 | 0.0061 | 0.0026 |
| 18.0 | 0.20 | 0.00421 | 0.0257 | 0.0029 | 0.0022 | 45.0 | 0.20 | 0.00421 | 0.0302 | 0.0049 | 0.0026 |
| 18.0 | 0.20 | 0.00750 | 0.0433 | 0.0065 | 0.0049 | 45.0 | 0.20 | 0.00750 | 0.0310 | 0.0057 | 0.0027 |
| 18.0 | 0.40 | 0.00042 | 0.0382 | 0.0055 | 0.0020 | 45.0 | 0.40 | 0.00133 | 0.0347 | 0.0072 | 0.0024 |
| 18.0 | 0.40 | 0.00075 | 0.0391 | 0.0051 | 0.0030 | 45.0 | 0.40 | 0.00237 | 0.0387 | 0.0070 | 0.0021 |
| 18.0 | 0.40 | 0.00133 | 0.0405 | 0.0050 | 0.0027 | 45.0 | 0.40 | 0.00421 | 0.0215 | 0.0046 | 0.0016 |
| 18.0 | 0.40 | 0.00237 | 0.0275 | 0.0037 | 0.0019 | 45.0 | 0.40 | 0.00750 | 0.0273 | 0.0053 | 0.0027 |
| 18.0 | 0.40 | 0.00421 | 0.0328 | 0.0045 | 0.0028 | 45.0 | 0.40 | 0.01330 | 0.0328 | 0.0067 | 0.0043 |
| 18.0 | 0.40 | 0.00750 | 0.0312 | 0.0042 | 0.0029 | 45.0 | 0.65 | 0.00133 | 0.0418 | 0.0081 | 0.0027 |
| 18.0 | 0.40 | 0.01330 | 0.0258 | 0.0049 | 0.0063 | 45.0 | 0.65 | 0.00237 | 0.0262 | 0.0058 | 0.0013 |
| 18.0 | 0.65 | 0.00042 | 0.0543 | 0.0074 | 0.0051 | 45.0 | 0.65 | 0.00421 | 0.0294 | 0.0061 | 0.0028 |
| 18.0 | 0.65 | 0.00075 | 0.0497 | 0.0064 | 0.0037 | 45.0 | 0.65 | 0.00750 | 0.0240 | 0.0054 | 0.0026 |
| 18.0 | 0.65 | 0.00133 | 0.0360 | 0.0046 | 0.0028 | 45.0 | 0.65 | 0.01330 | 0.0199 | 0.0045 | 0.0016 |
| 18.0 | 0.65 | 0.00237 | 0.0439 | 0.0056 | 0.0038 | 45.0 | 0.65 | 0.02370 | 0.0220 | 0.0060 | 0.0025 |
| 18.0 | 0.65 | 0.00421 | 0.0272 | 0.0038 | 0.0026 | 45.0 | 0.90 | 0.00237 | 0.0291 | 0.0094 | 0.0022 |
| 18.0 | 0.65 | 0.00750 | 0.0251 | 0.0038 | 0.0025 | 45.0 | 0.90 | 0.00421 | 0.0204 | 0.0072 | 0.0013 |
| 18.0 | 0.65 | 0.01330 | 0.0196 | 0.0044 | 0.0032 | 45.0 | 0.90 | 0.00750 | 0.0088 | 0.0041 | 0.0005 |
| 18.0 | 0.90* | 0.00075 | 0.0397 | 0.0066 | 0.0041 | 45.0 | 0.90 | 0.01330 | 0.0201 | 0.0078 | 0.0015 |
| 18.0 | 0.90* | 0.00133 | 0.0370 | 0.0065 | 0.0037 | 45.0 | 0.90 | 0.02370 | 0.0031 | 0.0032 | 0.0004 |
| 18.0 | 0.90* | 0.00237 | 0.0330 | 0.0057 | 0.0028 | 75.0 | 0.10 | 0.00237 | 0.0453 | 0.0090 | 0.0047 |
| 18.0 | 0.90* | 0.00421 | 0.0205 | 0.0044 | 0.0014 | 75.0 | 0.10 | 0.00421 | 0.0610 | 0.0137 | 0.0088 |
| 18.0 | 0.90* | 0.00750 | 0.0199 | 0.0056 | 0.0019 | 75.0 | 0.20 | 0.00237 | 0.0341 | 0.0073 | 0.0037 |
| 18.0 | 0.90* | 0.01330 | 0.0180 | 0.0062 | 0.0016 | 75.0 | 0.20 | 0.00421 | 0.0407 | 0.0071 | 0.0035 |
| 28.0 | 0.04 | 0.00075 | 0.0476 | 0.0050 | 0.0048 | 75.0 | 0.20 | 0.00750 | 0.0312 | 0.0073 | 0.0032 |
| 28.0 | 0.04 | 0.00133 | 0.0407 | 0.0051 | 0.0056 | 75.0 | 0.40 | 0.00237 | 0.0444 | 0.0120 | 0.0029 |
| 28.0 | 0.10 | 0.00075 | 0.0416 | 0.0060 | 0.0044 | 75.0 | 0.40 | 0.00421 | 0.0405 | 0.0096 | 0.0037 |
| 28.0 | 0.10 | 0.00133 | 0.0388 | 0.0056 | 0.0034 | 75.0 | 0.40 | 0.00750 | 0.0236 | 0.0063 | 0.0020 |
| 28.0 | 0.10 | 0.00237 | 0.0414 | 0.0058 | 0.0034 | 75.0 | 0.40 | 0.01330 | 0.0318 | 0.0080 | 0.0031 |
| 28.0 | 0.10 | 0.00421 | 0.0347 | 0.0064 | 0.0072 | 75.0 | 0.65 | 0.00237 | 0.0224 | 0.0075 | 0.0016 |
| 28.0 | 0.20 | 0.00075 | 0.0385 | 0.0052 | 0.0023 | 75.0 | 0.65 | 0.00421 | 0.0243 | 0.0072 | 0.0018 |
| 28.0 | 0.20 | 0.00133 | 0.0303 | 0.0039 | 0.0022 | 75.0 | 0.65 | 0.00750 | 0.0314 | 0.0079 | 0.0027 |
| 28.0 | 0.20 | 0.00237 | 0.0306 | 0.0039 | 0.0021 | 75.0 | 0.65 | 0.01330 | 0.0212 | 0.0056 | 0.0025 |
| 28.0 | 0.20 | 0.00421 | 0.0354 | 0.0045 | 0.0030 | 75.0 | 0.65 | 0.02370 | 0.0252 | 0.0083 | 0.0026 |
| 28.0 | 0.20 | 0.00750 | 0.0434 | 0.0096 | 0.0043 | 75.0 | 0.90 | 0.00421 | 0.0234 | 0.0104 | 0.0020 |
| 28.0 | 0.40 | 0.00075 | 0.0476 | 0.0074 | 0.0037 | 75.0 | 0.90 | 0.00750 | 0.0109 | 0.0066 | 0.0013 |
| 28.0 | 0.40 | 0.00133 | 0.0435 | 0.0063 | 0.0025 | 75.0 | 0.90 | 0.01330 | 0.0145 | 0.0082 | 0.0019 |
| 28.0 | 0.40 | 0.00237 | 0.0337 | 0.0050 | 0.0029 | 75.0 | 0.90 | 0.02370 | 0.0093 | 0.0062 | 0.0011 |

**Table 3:** The quantity $x_{\mathbb{P}} F_2^{D(3)}$ (cont'd).